

SKELETAL KINEMATIC MEASUREMENT
USING MODEL-IMAGE REGISTRATION AND MECHANICAL CONSTRAINTS

By

SHANG MU

A DISSERTATION PRESENTED TO THE GRADUATE SCHOOL
OF THE UNIVERSITY OF FLORIDA IN PARTIAL FULFILLMENT
OF THE REQUIREMENTS FOR THE DEGREE OF
DOCTOR OF PHILOSOPHY

UNIVERSITY OF FLORIDA

2010

© 2010 Shang Mu

ACKNOWLEDGMENTS

I wish to express sincere appreciation to Dr. Banks, my advisor, who gave me enormous support throughout my quest. I thank J.D. Yamokoski for his preliminary work, discussion on the design of the software framework, and general support on my work. I thank Nick Dunbar for building the bi-plane calibration cube and for his help in the bi-plane experiment of natural joints and in various other situations. I thank Brody Huval for writing the bi-plane calibration program with Nick's help, Roshni Marballi, Michael DesRosiers, and Kyle Houston for performing measurements, and Brian Maas for running statistics.

Special thanks go to my father, who fostered my enthusiasm in science.

TABLE OF CONTENTS

	<u>page</u>
ACKNOWLEDGMENTS.....	3
LIST OF TABLES.....	6
LIST OF FIGURES.....	7
LIST OF ABBREVIATIONS.....	8
ABSTRACT.....	9
CHAPTER	
1 INTRODUCTION.....	11
Background.....	11
Research Overview.....	14
A Quantitative Evaluation of the Influences on the Accuracy from Various Effects.....	14
Articular Constraints.....	15
Passive Elastic Joint Constraints.....	15
2 INFLUENCE OF BONE MODEL, NUMBER OF IMAGE PLANES, AND OBSERVERS ON THE ACCURACY OF JOINT KINEMATICS FROM RADIOGRAPHIC MODEL-IMAGE REGISTRATION.....	18
Introduction.....	18
Methods.....	20
Results.....	23
Discussion.....	25
3 ARTICULAR CONSTRAINTS.....	34
Introduction.....	34
Methods.....	36
Penetration Computation Algorithm.....	36
Image Comparison Metric.....	38
Optimizers and Cost Functions.....	38
Experimental Setup.....	40
Results.....	42
Discussion.....	42
Acknowledgements.....	45
4 LIGAMENT-LIKE JOINT CONSTRAINTS.....	49

Introduction	49
Methods	50
Data sets	50
Registration method	51
Performance evaluation.....	54
Results.....	55
Discussion	56
5 CONCLUSION.....	62
APPENDIX: OPTIMIZER PARAMETER VALUES	64
LIST OF REFERENCES	65
BIOGRAPHICAL SKETCH.....	69

LIST OF TABLES

<u>Table</u>		<u>page</u>
2-1	Actual range of motion in the 10 image pairs per joint, measured using bi-plane bead registrations.	30
2-3	RMS differences between bead and bone models for all observers and single- and bi-plane measurements.....	30
2-4	Average difference of each observer from the mean of all observers, for all image data, including single- and bi-plane measurements, and bead and bone models.	31
2-5	RMS difference between observers for bi-plane registration of bead models.....	31
2-6	RMS differences between bi-plane bead model measurements and single-plane bead model measurements.	31
2-7	RMS differences between bi-plane bead model measurements and bi-plane bone model measurements.	32
2-8	RMS differences between bi-plane bead model measurements and single-plane bone model measurements.	32
3-1	Success rates and RMS registration errors for three methods with and without the contact function penalty or constraint.	46
4-1	Success rates and the relative pose RMS deviations for two datasets with and without contact and/or ligament penalty.	59
A-1	Particle swarm pattern search parameter values.....	64
A-2	RALG optimizer parameter values.....	64
A-3	Levenberg-Marquardt nonlinear least squares optimizer parameter values.	64

LIST OF FIGURES

<u>Figure</u>		<u>page</u>
1-1	Models of bones or implants can be registered with their radiographic projections to provide accurate measures of dynamic 3D motion.....	17
1-2	Basic 3D-2D registration process for measuring 3D poses from 2D image(s)....	17
2-1	Biplane registration of elbow bone models.	33
3-1	Knee implant models matched to the fluoroscopic image to measure their spatial poses.....	47
3-2	Illustration of inside/outside determination for articulating polygonal surfaces. ..	47
3-3	Standard deviation of the errors in the measured relative joint position and joint angles.	48
3-4	Mean errors in the measured relative joint position and joint angles.	48
4-1	The symmetric view problem involves nearly equivalent projections of symmetric objects.....	60
4-2	Coordinate system definition for the femoral and tibial implant models.....	60
4-3	Silhouette of ill-registered tibia component models.	61
4-4	An image from Dataset B.	61

LIST OF ABBREVIATIONS

CT	Computed tomography.
DOF	Degree of freedom.
LSQ	Least squares (optimization).
MR	Magnetic resonance (imaging).
Pswarm	Particle swarm pattern search algorithm.
RMS	Root mean square.

Abstract of Dissertation Presented to the Graduate School
of the University of Florida in Partial Fulfillment of the
Requirements for the Degree of Doctor of Philosophy

SKELETAL KINEMATIC MEASUREMENT
USING MODEL-IMAGE REGISTRATION AND MECHANICAL CONSTRAINTS

By

Shang Mu

December 2010

Chair: Scott A. Banks
Major: Mechanical Engineering

Skeletal kinematic measurement using model-image registration has been practiced for more than fifteen years and proven useful elucidating the dynamic function of human joints with and without arthroplasty. However, technical complexity and the time consuming nature of the analysis have restricted utilization to a few research groups, and improvements on the methods have been few. To facilitate the use of model-image registration for skeletal kinematics studies and to enhance research collaboration, we have been developing JointTrack, an open-source, expandable software platform for radiographic model-image registration. Using this software, in the first part of this dissertation, we evaluate the influence of bone geometry, number of image planes, and the human operator on the accuracy of joint kinematics measurements, and identify limitations and weaknesses in the methods.

In the later parts of this dissertation, we investigate new techniques to improve measurement accuracy and reduce human labor. Compared to bi-plane (stereo) measurement, single-plane setup dominates the field due to physical constraint or equipment availability, but is intrinsically less accurate to a degree that limits its application, and delivers many difficulties to the registration process. Improvement on

the accuracy in single-plane measurement was achieved by incorporating contact constraint into the registration process. Further incorporation of ligament-like force models productively improved registration success rate, decreasing the need for human intervention in initial setup and/or late-stage validation and correction.

CHAPTER 1 INTRODUCTION

Background

“Register: 5.b. v.trans. To position with precision, in order to ensure an exact correspondence of parts; to align.” – The Oxford English Dictionary (<http://dictionary.oed.com/>, accessed November 2010).

Model-image registration (Fig. 1-1) for the measurement of dynamic skeletal motion has been used for orthopaedic research since 1991 (Banks et al., 1991). In this technique, a 3D model of a bone or implant is projected onto a digitized radiographic image and its 3D pose is adjusted until the projection matches the image. The technique gained popularity due to its non-invasive nature, accuracy, and capability of obtaining measurements for dynamic *in vivo* (i.e. real life) activities. Measurement precision on the order of 1mm translation or 1° rotation provides information that is useful to improve understanding of dynamic joint instability (e.g. Yamaguchi et al., 2009), improvement of joint replacement designs (e.g. Banks et al., 1997), and dynamic simulation of joint mechanics (e.g. Zhao et al., 2007).

In this technique, X-ray images of a moving joint are first obtained from systems capable of continuously capturing images, known generally as fluoroscopy systems. Given the 3D model of an object (a bone or an implant) and the radiographic projection parameters, a computer simulated perspective projection of the 3D model is generated and compared with the actual x-ray images using an image similarity measure. Given a single frame radiographic image and a 3D model, a search procedure, often a numerical optimization routine, is then used to find the best set of 3D model pose parameters that maximize the similarity measure (Fig. 1-2). This procedure is repeated for each bone or implant and for each frame to obtain the complete temporal kinematics of the objects.

Numerous groups developed measurement tools based upon model-image registration and applied these in studies of natural and prosthetic joints. In these reports, generation of perspective projection images mostly have been standard computer graphics routines using surface models of bone or implants (Banks and Hodge, 1996; Zuffi et al., 1999; Valstar et al., 2001; Mahfouz et al., 2003; Li et al., 2004; Yamazaki et al., 2004; Hirokawa et al., 2008; Prins et al., 2010), and recent reports have used digital reconstructed radiographs (DRR) from CT volumes (You et al., 2001; Tang et al., 2004). Image comparison metrics have been based on correspondence of image edges (Banks and Hodge, 1996; Valstar et al., 2001; Yamazaki et al., 2004; Hirokawa et al., 2008), weighted edge and grayscale correlation (Mahfouz et al., 2003), general normalized correlation (You et al., 2001), and gradient correlation (Tang et al., 2004). A different class of methods using 3D distance maps, based on efficient ray-tracing techniques, also have been reported (Lavallee and Szeliski, 1995; Zuffi et al., 1999). A wide range of optimization algorithms and numerical solvers have been utilized for model-image registration, including Levenberg–Marquardt nonlinear least squares algorithm (Zuffi et al., 1999), combined Nelder–Mead down-hill simplex and simulated annealing method (Mahfouz et al., 2003), feasible sequential quadratic programming (FSQP) (Valstar et al., 2001), Durand-Kerner method (Yamazaki et al., 2004), simple searches within low-dimension precomputed shape-libraries (Banks and Hodge, 1996; Hirokawa et al., 2008), and interactive manual matching by a human operator using solid-modeling software (Li et al., 2004). The majority of these reports provide careful evaluations of measurement accuracy, typically for a specific joint of interest or specific research application. However, none of these reports have quantified measurement

accuracy with multiple factors and observers (human operators) using consistent image sets on multiple natural joints.

Kinematic measurement accuracy for mode-image registration techniques varies little with the details of the image processing and optimization algorithms, but is affected significantly by single-plane or bi-plane imaging techniques. Single-plane imaging is monocular vision, which is fundamentally insensitive for translations along the viewing axis (Z-axis in our standard coordinate system). Bi-plane imaging techniques capture images from two views simultaneously, providing stereo visualization and more uniform and precise measurements than single-plane imaging. However, bi-plane systems often have very limited space within which an activity can be performed, they double the x-ray exposure and are not generally available in hospitals. Single-plane imaging systems are found in every hospital, and so are readily available for dynamic imaging. However, there have been few reports of methods that improve single-plane registration precision (Yamazaki et al., 2004).

The robustness of kinematic measurement techniques rarely has been reported. Mahfouz et al. (2003) reported 50% registration success for knee replacement implants when the initial guess was 16mm from the in-plane solution, 128mm from the out-of-plane solution and 16° from the rotation solution. Their registration success rate increased to over 90% when the initial guesses were within 4mm, 32mm and 4° , respectively. The fact remains that all reported techniques for skeletal kinematic analysis rely on an operator-provided guess to start the registration process for every image in the sequence. The labor-intensive nature of these measurements is a significant factor limiting their use in research and preventing their clinical use.

Image quality and object shape (bone or implant) strongly affect model-image registration success rates. For this reason, some bones are extremely difficult to measure. Patella kinematics, as an example, are hard to measure due to the round shape, small size and the poor image contrast of the patella, and have only recently been measured using a bi-plane x-ray system (Bey et al., 2008). The bones of the foot/ankle, the talus and calcaneus in particular, also present measurement challenges due to their oblong rounded shapes and overlapping joints (poor contrast images), yet there is strong interest to quantify foot/ankle motion in pathologic feet during walking.

In this dissertation, we evaluated the performance of a basic model-image registration method that has been used by our group and identify limitations and weaknesses in the method. With these limitations clearly identified, we present two approaches to enhance accuracy and success rates for 3D-to-2D model-image registration.

Research Overview

A Quantitative Evaluation of the Influences on the Accuracy from Various Effects

Bi-plane images were taken from four different natural joints *in vitro*. Registration was performed by multiple human operators for four different conditions: bi-plane images with models of metallic beads implanted in the bones, bi-plane images with 3D bone models, single-plane images with bead models and single-plane images with 3D bone models. Accuracy for each condition was quantified and analyzed with statistical models. We specifically evaluated the influence of registration model (bones versus beads), number of image planes (bi-plane versus single-plane), and the effect of human observers on the accuracy of joint kinematics from radiographic model-image registration, and the results are documented and discussed in Chapter 2.

Articular Constraints

Contact is the most important aspect of human joints, but is rarely used in model-image registration methods to improve accuracy (Hirokawa et al., 2008, Prins et al., 2010). Hirokawa et al. (2008) incorporated contact into the registration algorithm by solving simultaneous equations for the contact point(s). Because this method requires the articulating surfaces to be described in parametric equations, different joints need to be handled differently, and it is difficult to apply the method to complex contacts, especially natural joints without prostheses. Prins et al. (2010) reported a technique similar to the one proposed in this dissertation. However, neither of these two methods can handle deformation, wear, or inaccuracy of the 3D surface models. The method proposed in Chapter 3 addresses these issues naturally. In brief, the method integrates contact constraints into the model-image registration process to improve measurement in the out-of-plane direction in single-plane registration. In addition, the contact constraint dramatically shrinks the configuration space of the optimization problem and therefore increases the rate of successful registrations in certain cases.

Passive Elastic Joint Constraints

The motions within human joints are constrained by the ligaments and soft-tissues surrounding each joint. These soft-tissues, even when damaged or diseased, define a passive envelope of possible motions. Knowledge of this passive envelope might be useful to constrain the model-image registration process to evaluate only physiologically feasible joint configurations. In Chapter 4, we incorporate into the model-image registration process passive joint constraints modeled as restoring ligament forces. These constraints reduced the need for accurate initial guesses and significantly increased the rate of successful registrations. In particular, false extrema due to object

symmetry were effectively avoided using such constraints. These ligament-like constraints also have the potential reduce the requirements for careful human review of each registration result. We are not aware of any existing reports of similar methods.

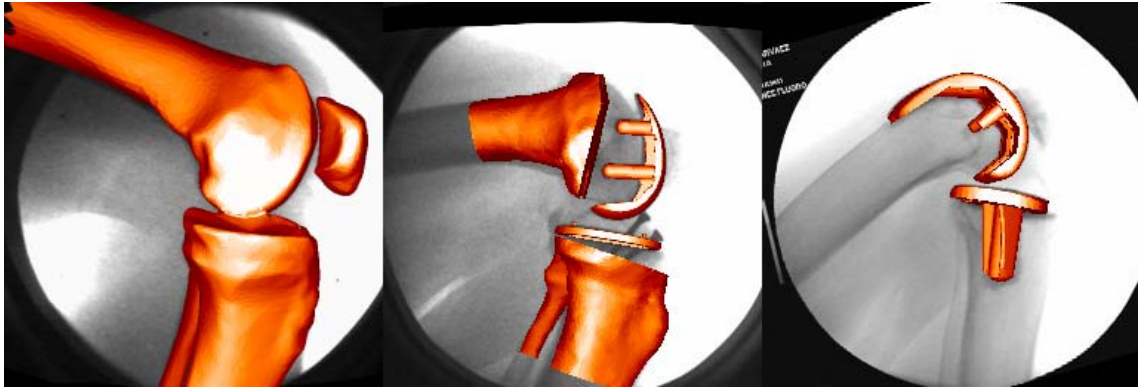


Figure 1-1. Models of bones or implants can be registered with their radiographic projections to provide accurate measures of dynamic 3D motion.

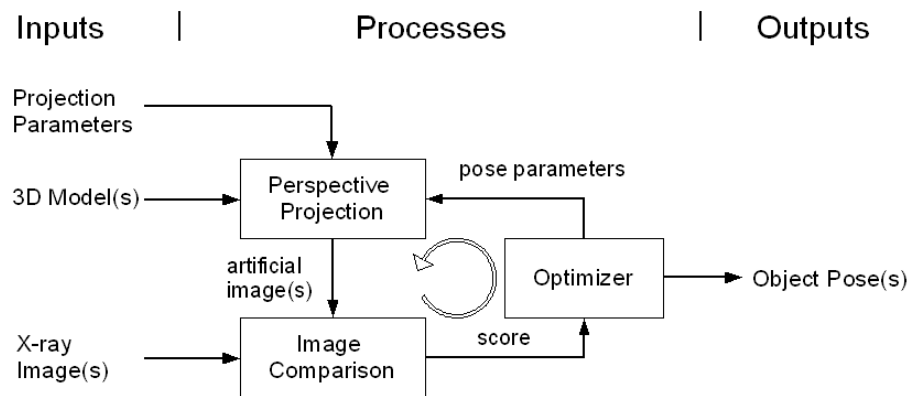


Figure 1-2. Basic 3D-2D registration process for measuring 3D poses from 2D image(s).

CHAPTER 2
INFLUENCE OF BONE MODEL, NUMBER OF IMAGE PLANES, AND OBSERVERS
ON THE ACCURACY OF JOINT KINEMATICS FROM RADIOGRAPHIC MODEL-
IMAGE REGISTRATION

Introduction

Model-image registration for in vivo skeletal kinematic measurement has become a very popular research tool since it was first reported in 1991 (Banks and Hodge, 1992). For example, an *ISI Web of Knowledge* keyword search for the terms “fluoro* and kinematics” yields 106 relevant peer-reviewed papers in archival journals from January 2008 to October 2010. There are a wide range of techniques implemented to perform these measurements, but they all share the common elements of (1) one or more radiographic projections with measured geometry, (2) three-dimensional models of one or more moving bones or implants, and (3) a procedure to register the models with the radiographic projections by computer synthesis of candidate projections, comparison with a metric and iterative numerical refinement (e.g. Banks and Hodge, 1996; You et al., 2001; Kaptein et al., 2003; Mahfouz et al., 2003). These techniques have been applied to quantify in vivo the movement of, for example, total knee replacements (e.g. Banks et al., 1997; Stiehl et al., 1999; Zuffi et al., 1999; Kaptein et al., 2003; Yamazaki et al., 2004), natural knees (e.g. Komistek et al., 2003; Li et al., 2007; Tashman et al., 2007; Moro-oka et al., 2008), natural and replaced shoulders (Kon et al., 2008; Nishinaka et al., 2008), hip replacements (Komistek et al., 2002; Tanino et al., 2008), natural and replaced ankles (Yamaguchi et al., 2009), elbows (Matsuki et al., 2010) and spinal vertebrae (Wang et al., 2008; McDonald et al., 2010). Several studies have reported careful evaluations of measurement accuracy with knee implants (e.g. Banks and Hodge, 1996; Kaptein et al., 2003; Mahfouz et al., 2003;

Kaptein et al., 2007), yet there remain many issues associated with model-image registration measurement techniques for joints without implants that have not been addressed. Important questions remain concerning the relative accuracy of single-projection and stereo measurements, the influence of bone shape on measurement accuracy, and how multiple users affect measurement precision.

Model-image registration based measurements have the potential to provide useful and clinically relevant information if sufficiently well developed. Technical challenges for a clinical implementation will include the need to automate the measurement, to characterize the measurement applied to different joints with and without implants, and to minimize the influence of a human operator on the measurement procedure. Although not yet a fully automatic and robust measurement capability, it remains worthwhile to quantify present technical capabilities to inform research efforts and to guide priorities for future developments. In this study, we sought to answer the following three questions:

1. How much does joint kinematics measurement accuracy decrease using a single-plane imaging technique compared to a stereo imaging technique?
2. How is joint kinematics measurement accuracy affected by the shape model, i.e. models of bones versus models of discrete marker clusters?
3. How is joint kinematics measurement accuracy affected by the user?

Answers to these questions put into perspective reports currently appearing in the research literature and suggest how development efforts should be prioritized to reach a clinically useful in vivo skeletal kinematic measurement capability.

Methods

A stereo flat-panel radiographic imaging system was used for this study (Allura Xper FD20/20, Philips Medical Systems B.V.). All images were obtained at 15 frames per second with 3ms exposures. Beam energy and current were adjusted for each case prior to recording dynamic trials. The photogrammetric geometry of the two image systems was determined using a cubic three-dimensional (3D) calibration object consisting of plastic plates with embedded metallic spheres. The 3D sphere locations were determined by merging reconstructed bead locations from a pair of CT scans acquired with the calibration object in two orthogonal orientations relative to the scan direction. Repeated calibrations yielded image-plane bead reconstruction residuals of 0.3mm.

One lower extremity and one forequarter cadaveric specimen were properly obtained and prepared for the study. Three to five metallic beads (2mm Pb) were placed in the scapula, proximal and distal humerus, radius, ulna, femur, patella, proximal and distal tibia, talus and calcaneus. No skin or soft-tissue was removed from the specimens. CT scans with 0.5mm slice thickness were acquired for the specimens (Sensation 16, Siemens) and the 3D surface geometries of the bones and the implanted beads were reconstructed using open-source software (Yushkevich et al., 2006). The 3D models were aligned with standard joint reference systems (Moro-oka et al., 2008; Nishinaka et al., 2008; Yamaguchi et al., 2009; Matsuki et al., 2010). The knee, lower shank and foot, and forequarter specimens were mounted to radiolucent (x-ray transparent) fixtures such that each joint could be taken through a range of motion during radiographic observation.

Image detectors were aligned with each joint so that one plane was a lateral or antero-posterior projection as would commonly be used for a single-plane observation. The other detector was aligned to obtain a clear view of the moving joint with an angular separation of 50°-60° from the first detector. Image sequences were obtained for each joint as it was manually moved through a range of motion that included primary and secondary rotations of the joint. For each joint a group of ten image pairs were chosen to cover the joint range of motion and these images were placed in a randomly ordered sequence.

Model-image registration was performed using custom open-source software with capability for both single-plane and stereo image analysis (JointTrack, www.sourceforge.net/projects/jointrack). The user adjusted grayscale parameters and edge enhancement (Canny, 1986) for individual images or the entire sequence. The user selected a model and manually positioned it in 3D space using the mouse and keyboard while viewing synthetic radiographic projections and a 3D viewing window showing the relative position of all the bones in the joint (Fig. 2-1). With this initial pose as a starting point, the model-image registration was iteratively refined using a simulated annealing global optimization routine (Kirkpatrick et al., 1983; Goffe et al., 1994) and a cost-function summing the cross-correlations of the grayscale and edge-detected (Canny, 1986) versions of the actual and synthesized radiographic projections.

At least three, and in most cases four, human users performed the model-image registration measurements for each image sequence. Users ranged from orthopaedic surgeons who were very familiar with the anatomy and experienced using the software,

to undergraduate engineering students with little anatomic familiarity and only basic instruction in how to use the measurement software. Users performed the model-image measurement process independently four times for each image sequence with the following conditions:

1. Stereo images with 3D models of the bones with the metallic beads.
2. Stereo images with 3D bone models without beads.
3. Single-plane images with 3D models of the bones with the metallic beads.
4. Single-plane images with 3D bone models without beads.

The resulting 3D bone kinematics were used to compute joint kinematics in the anatomic reference frames for the patellofemoral, tibiofemoral, tibiotalar, subtalar, glenohumeral, radiohumeral, and radioulnar joints. Mean values were compared using an analysis of variance model (The R Project for Statistical Computing, www.r-project.org) without interaction between factors:

$$y_{ijkl} = \bar{y}_{\dots} + \bar{y}_{i=n_planes} + \bar{y}_{j=bead_or_bone} + \bar{y}_{observer_k} + \bar{y}_{frame_l} + \varepsilon(N(0, \sigma^2)) \quad (\text{Eq. 2-1})$$

where y is any measured pose parameter, the bar on top means taking the average value (e.g. \bar{y}_{\dots} is the total mean of all the measured values), and $\varepsilon(N(0, \sigma^2))$ is a normally distributed random error. Average kinematics determined from bi-plane images registered with 3D bead models were taken as reference values, and relative measurement errors σ^2 were determined for the other cases. Measurement precision (the reciprocal of the variance) within each combination of conditions (or factors) was determined from the computed differences from reference values, and factor effects were estimated using a generalized linear model with the gamma distribution:

$$s_{ijk}^2 = offset + \sigma_{i=n_planes}^2 + \sigma_{j=bead_or_bone}^2 + \sigma_{observer_k}^2 + \varepsilon \quad 1/s_{ijk}^2 \sim \Gamma(k, \theta) \quad (\text{Eq. 2-2})$$

where s_{ijk}^2 is the sample variance within each combination and each σ^2 is the variance due to a specific factor. Statistical significance was defined as a probability (p) of 0.05 or less. Root-mean-square errors due to each factor were constructed from the mean and estimated variance values. Based on clinician feedback, measurement errors greater than 1mm or 1° are considered noteworthy.

Results

The actual ranges of joint motion measured from the 10 image pairs of each joint are presented in Table 2-1. All joints demonstrated joint rotations greater than 25° about one or more axes, except the talocalcaneal joint.

Joint kinematics measurement accuracy was significantly worse for all single-plane measurements compared to all bi-plane measurements (Table 2-2). Five of eight joints showed differences of greater than 1mm in out-of-plane (Z-axis) translations comparing single-plane measurements to bi-plane measurements. In-plane translation measures were significantly different from the bi-plane measures in all eight joints, and in 5-of-8 cases these joints had significant out-of-plane translation differences. Only the talocalcaneal joint showed significant large (>1°) differences in the z-axis rotation (plantar/dorsiflexion). In general, the best single-plane results were obtained for the knee and elbow joints, with the shoulder and foot/ankle joints having larger differences from the reference measures.

Model type, 3D bones versus metallic beads, had a very strong influence on measurement accuracy (Table 2-3). Seven out of eight joints registered with 3D bone models showed differences greater than 1° (differences > 2° in six of eight joints) in the out-of-plane (X- and Y-axis) rotations compared to the reference data using implanted

metallic beads. In-plane (Z-axis) rotation differences, where statistically significant, were less than 1.2° for all joints. Significant differences in translations were less than 1mm for all joints, except for the out-of-plane (Z-axis) translation of the talocalcaneal joint.

For most joints there were not large differences ($>1\text{mm}$ or $>1^\circ$) due to the observer performing the measurement (Table 2-4). The exception to this finding was the talocalcaneal joint, where all six degrees of freedom showed significant differences of greater than 1mm or 1° . Three of eight joints showed interobserver differences greater than 1° for long-axis (Y-axis) rotations.

Direct comparisons of specific datasets provides additional useful information. We see sometimes large ($> 2\text{mm}$ or $>2^\circ$) RMS differences between observers performing the 3D pose measurement for the bi-plane bead dataset (Table 2-5). The largest average differences were observed for the talocalcaneal joint and for the Y-axis (long-axis) rotations. The tibiofemoral joint (knee) was most consistently measured.

Single-plane measures using the bead models showed large ($> 2\text{mm}$ or $>2^\circ$) RMS differences for the out-of-plane translations (Z) and rotations (X and Y), and were largest for the talocalcaneal joint (Table 2-6). The tibiofemoral joint showed the smallest differences contrasting the single- and bi-plane bead measurements.

Bi-plane and single-plane measurements using 3D bone models also showed large ($> 2\text{mm}$ or $>2^\circ$) RMS differences for the out-of-plane translations (Z) and rotations (X and Y), and were largest for the talocalcaneal joint (Tables 2-7 and 2-8). The RMS differences for the bi-plane bone measurements were generally smaller than those for the single-plane bone measures for the out-of-plane translations (Z) and rotations (X and Y), and similar for the in-plane translations (X and Y) and rotations (Z).

Discussion

Radiograph derived joint kinematic measurements have become a common and important research tool for joint biomechanics studies. Use of these techniques is rapidly expanding with the introduction of free open-source and commercial software. As the users of these tools shifts from the original developers to those who simply want to use the tools to perform measurements, it is increasingly important to establish expectations for measurement quality across the broad range of applications. In this study we sought to quantify joint kinematics measurement accuracy across a range of joints, imaging setups, and users. We confirmed that single-plane measures are not as accurate as bi-plane measures, especially for out-of-plane translations. We showed that out-of-plane rotations, in particular, are less accurate using bone models for registration compared to clusters of small spherical metallic markers. Long bones showed larger errors for measuring rotations about the long axis, except the knee, where the articular morphology has a rich shape compared to the proximal radius or humerus. Finally, we showed that interobserver differences can be significant, especially for out-of-plane rotations and for specific challenging joints. Beyond the specific findings, these data for different combinations of image planes, object models and observers provide a baseline assessment of registration performance with which future developments can be compared.

The study has several limitations that are important to recognize. First, we used only one software tool and employed a global numerical optimizer to perform the registrations. We did not refine the global optimizer results with a gradient-based routine afterward. We believe these results are representative of a very basic manual-plus-

numerical registration procedure, and serve to highlight areas where further refinement of registration techniques and numerical algorithms might best be targeted for specific joints. The results do not suggest that other reported registration techniques are necessarily inferior or superior. Second, the study images were generated using a bi-plane imaging system that pulsed the two x-ray tubes in an evenly alternating fashion. Since the images were not simultaneously acquired there will be errors introduced in the bi-plane kinematic measurement. We sought to minimize this source of error by slowly moving the test specimens during image capture. Finally, the upper extremity specimen was not attached to the thorax, so the images lacked the ribs and chest anatomy present in vivo.

Tang et al. (Tang et al., 2004) assessed the accuracy of measuring patellofemoral joint kinematics using a cadaver setup with single- and bi-plane imaging, and performed registration with bone models and bead-based models. When comparing the single-plane measures to the bi-plane measures using bead-based models, they found RMS differences of 1.6° for rotations, 1.6mm for in-plane translations, and 1.3mm for out-of-plane translations. We found RMS differences of 1.2° for rotations, 0.8mm for in-plane translations, and 5.9mm for out-of-plane translations (Table 2-6). When comparing the single-plane measures to the bi-plane measures using projected 3D bone models, they found RMS differences of 2.1° for rotations, 1.8mm for in-plane translations, and 2.0mm for out-of-plane translations. We found RMS differences averaging 2.4° for rotations, 0.9mm for in-plane translations, and 5.1mm for out-of-plane translations (Table 2-8). Our results are mostly comparable to Tang et al., except our out-of-plane translation errors are much larger. Tang et al. used approximately double the number of metallic

beads in each bone for the bead-model registrations, and used digital-reconstructed-radiograph (DRR) projections for the bone-model registrations. These technical differences likely account for Tang's greater out-of-plane translation accuracy.

Bey et al. (2008) compared bi-plane measurements of patellofemoral kinematics and found 0.4mm RMS differences for all translations and 0.9° differences for all rotations comparing bead- and bone-model based measures. We found average differences of 0.8mm for all translations and 2.2° for all rotations. Again, use of a DRR projection method for bone-model registration appears to provide superior bi-plane bone-model registration results.

Morooka et al. (Moro-oka et al., 2007) reported an assessment of model-image registration using synthetic images and found best-case registration errors for the tibiofemoral joint of 0.5mm for in-plane translations, 2mm for out-of-plane translations, and 0.5° for all rotations. Tsai et al. (Tsai et al., 2010) recently reported the development of an image-only registration method for tracking the knee bones using fluoroscopy. They report experimentally measured accuracy of 0.8mm for in-plane translations, 3.1mm for out-of-plane translations and 1.1° for all rotations. Comparing our single-plane bone model results to the reference data (Table 2-8), we found RMS differences of 0.7mm for in-plane translations, 2.8mm for out-of-plane translations, and an average of 1.3° for all rotations; strikingly similar to Tsai's results. These results confirm that even simple methods with user supplied initial guesses can provide clinically useful kinematic measures for 5 of the 6 degrees of freedom for the tibiofemoral joint. Our results confirm that additional work is required to improve the out-of-plane translation measurement, and to further automate the registration process.

Bey et al. (2006) validated a bi-plane model-based registration technique for the shoulder (glenohumeral joint) in comparison to a bead-based bi-plane technique. Comparing bone-model and bead-based registrations, they found average RMS errors of 0.385mm and 0.25° for the scapula, and 0.374mm and 0.47° for the humerus. Assuming these errors are uncorrelated, RMS errors for measuring scapulohumeral kinematics would be approximately 0.8mm and 0.75°. Comparing the bi-plane bone model results with the bi-plane bead model results, we found RMS differences averaging 0.8mm and 2.0° for scapulohumeral kinematics. Bey et al. used a similar number of beads in each bone, but used a DRR projection method for the bone model registrations. This more realistic model projection method likely accounts for the higher rotational accuracy.

There appear to be no reports of accuracy assessment for single-plane model-image registration with the shoulder, elbow or hindfoot. Our data will provide basic observations on measurement performance with these joints. Measurement results for the elbow showed translation errors of less than 2mm, but large long-axis (Y-axis) rotation errors were observed. This finding should not be surprising as both the radius and ulna present as long cylindrical objects with few shape features to change the projection with long-axis rotation (Fig 2-1). Single-plane studies will benefit from visualization of the entire forearm to the wrist, where the radius and ulna are not cylindrical.

Measurement results for hindfoot kinematics (tibiotalar and talocalcaneal joints) showed typical translation errors in excess of 1mm and typical out-of-plane rotation errors greater than 3° (Table 2-2). These measure are poor compared to the knee joint,

and are large relative to the range of joint rotations (Table 2-1). Future efforts to measure hindfoot kinematics with single-plane registration techniques will need to incorporate surface interactions and, perhaps, ligament-like constraints to improve measurement accuracy.

There were statistically significant differences in the kinematics measured by different observers for every joint and for most degrees of freedom. The talocalcaneal joint was notable for these interobserver differences. These findings underscore the importance of developing and using more capable optimization routines and registration procedures to eliminate the effect of the initial pose estimate on the optimized pose.

This study provides a comprehensive assessment of model-image registration performance for eight joints considering the number of image planes, the registration model and interobserver variability. These observations highlight where simple registration methods currently provide measures useful for research or clinical application, and point out many cases where technical improvements are required. These data will provide a useful reference for assessing the utility of new registration techniques for quantifying 3D bone kinematics.

Table 2-1. Actual range of motion in the 10 image pairs per joint, measured using bi-plane bead registrations.

Joint	X translation (mm)	Y translation (mm)	Z translation (mm)	X Rotation (deg)	Y Rotation (deg)	Z rotation (deg)
Patellofemoral	65	31	2	82	10	6
Tibiofemoral	16	3	4	124	2	22
Talocalcaneal	3	6	4	6	4	4
Tibiotalar	2	1	1	25	7	4
Radioulnar	2	1	4	6	11	136
Radiohumeral	1	4	2	12	10	139
Elbow (ulna/humerus)	2	1	4	6	11	136
Scapulohumeral	3	10	7	32	8	33

Table 2-2. RMS differences between bi-plane and single-plane measurements for all observers, and bead and bone models.

Joint	X translation (mm)	Y translation (mm)	Z translation (mm)	X Rotation (deg)	Y Rotation (deg)	Z rotation (deg)
Patellofemoral (n=3)	0.9 ^{*#}	0.3 [#]	3.7 [*]	-	-	-
Tibiofemoral (n=3)	-	0.6 [*]	2.3 ^{*#}	0.3 [*]	0.4 [*]	-
Talocalcaneal (n=4)	3.8 ^{*#}	3.4 ^{*#}	-	4.2 [*]	3.3 [*]	1.2 [*]
Tibiotalar (n=4)	0.3 [*]	1.0 ^{*#}	-	3.3 [*]	-	0.6 [*]
Radioulnar (n=4)	1.4 [*]	0.4 [*]	1.4 [*]	0.9 [*]	5.7 [*]	0.8 [*]
Radiohumeral (n=4)	0.2 [*]	0.3 [*]	-	-	-	0.5 [*]
Elbow (ulna/humerus) (n=4)	1.4 [*]	0.4 [*]	1.4 [*]	0.9 [*]	5.7 [*]	0.8 [*]
Scapulohumeral (n=3)	0.9 [*]	1.4 [*]	10.1 ^{*#}	2.3 [*]	1.1 [*]	-

** indicates a statistically significant difference in mean values compared to the reference measures.*

indicates a statistically significant difference in sample variance compared to the reference measures.

- indicates a statistically significant difference with reference measurements was not found.

Shaded cells highlight differences greater than 1mm or 1°.

Table 2-3. RMS differences between bead and bone models for all observers and single- and bi-plane measurements.

Joint	X translation (mm)	Y translation (mm)	Z translation (mm)	X Rotation (deg)	Y Rotation (deg)	Z rotation (deg)
Patellofemoral (n=3)	-	-	-	-	-	-
Tibiofemoral (n=3)	0.4 [#]	-	0.9 [*]	0.6 [*]	1.2 ^{*#}	0.5 ^{*#}
Talocalcaneal (n=4)	-	0.5 [#]	1.2 [*]	2.8 [#]	2.5 ^{*#}	-
Tibiotalar (n=4)	-	0.4 [*]	0.9 [*]	3.1 ^{*#}	4.7 ^{*#}	1.2 ^{*#}
Radioulnar (n=4)	0.9 [*]	0.5 [#]	-	-	3.3 [*]	0.3 [*]
Radiohumeral (n=4)	-	-	-	1.3 [*]	2.6 [#]	-
Elbow (ulna/humerus) (n=4)	0.9 [*]	0.5 [#]	-	-	3.3 [*]	0.3 [*]
Scapulohumeral (n=3)	-	0.2 [*]	-	1.1 [*]	2.0 ^{*#}	0.4 ^{*#}

Table 2-4. Average difference of each observer from the mean of all observers, for all image data, including single- and bi-plane measurements, and bead and bone models.

Joint	X translation (mm)	Y translation (mm)	Z translation (mm)	X Rotation (deg)	Y Rotation (deg)	Z rotation (deg)
Patellofemoral (n=3)	0.1*	-	0.6*	-	0.5*	0.3*
Tibiofemoral (n=3)	0.2*	0.1*	0.8*	-	0.2*	0.2*
Talocalcaneal (n=4)	1.7*	3.0*	1.5*	2.2*	2.8*	1.2*
Tibiotalar (n=4)	-	0.1*	0.3*	0.8*	0.6*	0.1*
Radioulnar (n=4)	-	0.4*	1.0*	0.5*	1.1*	-
Radiohumeral (n=4)	0.2*	0.2*	-	0.5*	0.8*	0.1*
Elbow (ulna/humerus) (n=4)	-	0.4*	1.0*	0.5*	1.1*	-
Scapulohumeral (n=3)	0.1*	0.2*	2.0*	0.3*	-	0.2*

Table 2-5. RMS difference between observers for bi-plane registration of bead models.

Joint	X translation (mm)	Y translation (mm)	Z translation (mm)	X Rotation (deg)	Y Rotation (deg)	Z rotation (deg)
Patellofemoral (n=3)	0.3	0.3	0.6	1.1	1.2	0.8
Tibiofemoral (n=3)	0.4	0.4	0.4	0.3	0.3	0.4
Talocalcaneal (n=4)	3.6	6.8	3.8	4.8	6.5	5.5
Tibiotalar (n=4)	0.7	0.3	0.6	0.9	1.5	1.0
Radioulnar (n=4)	1.2	0.5	1.7	0.5	3.6	0.5
Radiohumeral (n=4)	0.5	0.4	1.2	0.5	2.4	0.8
Elbow (ulna/humerus) (n=4)	1.2	0.5	1.7	0.5	3.6	0.5
Scapulohumeral (n=3)	0.4	0.5	0.7	0.8	1.6	0.4

Table 2-6. RMS differences between bi-plane bead model measurements and single-plane bead model measurements.

Joint	X translation (mm)	Y translation (mm)	Z translation (mm)	X Rotation (deg)	Y Rotation (deg)	Z rotation (deg)
Patellofemoral (n=3)	1.1	0.5	5.9	1.1	1.3	1.3
Tibiofemoral (n=3)	0.6	0.9	3.9	0.5	0.4	0.6
Talocalcaneal (n=4)	4.3	3.4	5.8	3.5	3.6	3.0
Tibiotalar (n=4)	0.8	1.5	4.1	3.6	1.9	1.1
Radioulnar (n=4)	1.8	1.2	3.5	3.1	6.4	1.1
Radiohumeral (n=4)	0.7	0.5	3.3	2.8	3.1	0.8
Elbow (ulna/humerus) (n=4)	1.8	1.2	3.5	3.1	6.4	1.1
Scapulohumeral (n=3)	1.7	2.1	11.0	2.0	1.5	0.5

Table 2-7. RMS differences between bi-plane bead model measurements and bi-plane bone model measurements.

Joint	X translation (mm)	Y translation (mm)	Z translation (mm)	X Rotation (deg)	Y Rotation (deg)	Z rotation (deg)
Patellofemoral (n=3)	0.4	0.4	1.4	2.2	3.2	1.2
Tibiofemoral (n=3)	0.7	0.5	1.0	0.7	1.5	0.9
Talocalcaneal (n=4)	3.7	6.8	3.5	8.5	4.5	5.6
Tibiotalar (n=4)	0.8	0.6	1.4	4.1	4.8	1.7
Radioulnar (n=4)	1.6	1.0	3.3	1.6	7.7	0.7
Radiohumeral (n=4)	0.7	0.7	4.5	1.4	5.8	0.8
Elbow (ulna/humerus) (n=4)	1.6	1.0	3.3	1.6	7.7	0.7
Scapulohumeral (n=3)	0.5	0.6	1.2	1.5	3.8	0.6

Table 2-8. RMS differences between bi-plane bead model measurements and single-plane bone model measurements.

Joint	X translation (mm)	Y translation (mm)	Z translation (mm)	X Rotation (deg)	Y Rotation (deg)	Z rotation (deg)
Patellofemoral (n=3)	1.3	0.6	5.1	3.3	2.6	1.3
Tibiofemoral (n=3)	0.6	0.7	2.8	1.1	1.9	0.8
Talocalcaneal (n=4)	4.3	3.4	3.2	7.3	7.6	2.9
Tibiotalar (n=4)	0.8	0.7	1.6	6.6	6.1	2.0
Radioulnar (n=4)	1.5	1.3	3.3	2.0	6.2	1.0
Radiohumeral (n=4)	0.7	0.7	2.0	3.1	3.7	1.0
Elbow (ulna/humerus) (n=4)	1.5	1.3	3.3	2.0	6.2	1.0
Scapulohumeral (n=3)	1.1	1.9	13.3	4.1	8.4	2.0

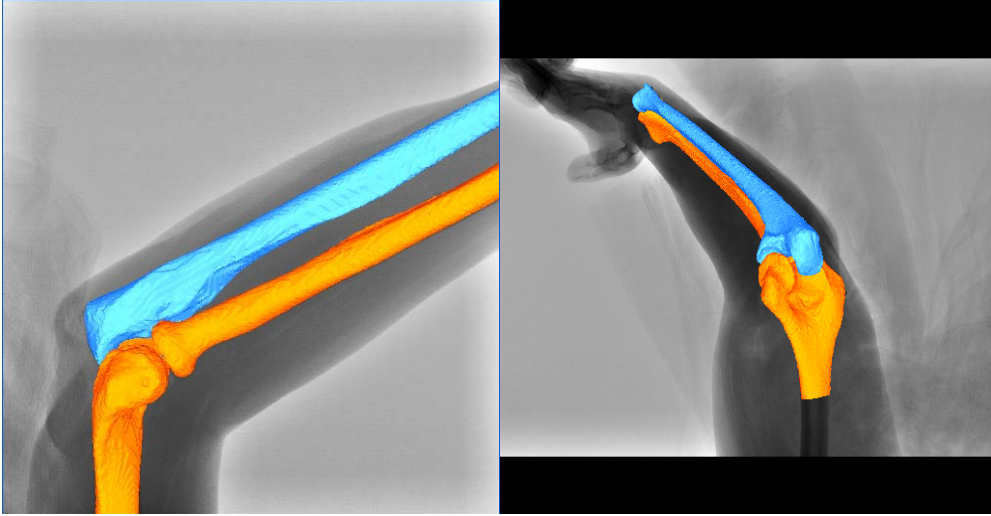


Figure 2-1. Biplane registration of elbow bone models.

CHAPTER 3 ARTICULAR CONSTRAINTS

Introduction

3D-to-2D model-image registration performed with radiographic images is an important tool for measuring in-vivo joint kinematics. It has been proven useful for the study of a number of clinical and research topics in a variety of joints, such as implant performance (Banks et al., 2005), pathological or natural joint mechanics (Yamaguchi et al., 2009; Matsuki et al., 2010), and contact model development (Fregly et al., 2005). Measurement uncertainty usually is on the order of 1mm or 1° for 5 of 6 degrees of freedom characterizing joint kinematics from a single-plane projection (e.g. Banks and Hodge, 1996; Zuffi et al., 1999). However, the same level of accuracy is not achieved in the out-of-plane direction. Bi-plane or stereoradiographic systems achieve better and more uniform accuracy, but they limit the viewing volume in which an activity can be performed, double subject x-ray exposures, increase cost, and are not available at many institutions. Thus, there remains strong incentive to improve the accuracy of single-plane measures for research and, ultimately, clinical joint kinematic assessments.

Hirokawa et al. (2008) incorporated an articular surface model into their registration method to improve out-of-plane measurement accuracy for total knee replacements. They added a system of ten constraint equations in fourteen variables to describe the points of contact between the tibia and femur and found numerically a solution that best satisfied their image-registration cost-function and articular constraint equations. Validation experiments with a robot manipulating knee replacement components reduced out-of-plane translation errors from approximately 5mm to less than 1mm.

Prins et al. (Prins et al., 2010) improved out-of-plane measurement accuracy by detecting collision between the femoral component and the tibial insert in total knee replacements. In their phantom study evaluation, accuracy was improved from 2.1mm to 0.1mm RMS translation in the out-of-plane direction, with no loss of accuracy in the other degrees of freedom when using accurate 3D implant models. In their method, pose estimation is first performed with the traditional image-matching-only method, and then a correction step with the inclusion of penetration detection is carried out to correct the out-of-plane translation.

In this chapter, we present a different approach to detect and compute a measure of articular contact or penetration. We incorporate an articular surface proximity measure with several optimization algorithms and compare the success rate and accuracy compared to a reference dataset. Compared to the methods of Hirokawa et al. or Prins et al., this method provides several potential advantages:

- Surface penetration can be quantified as depth, area, quasi-volume, or can be represented as an elastic foundation (Winkler, 1867). Surface separations also can be calculated within the same framework. Thus, a wide range of penalty functions or optimization constraints can be configured from the same basic method.
- Because explicit surface penetration/separation distances are computed, physically intuitive gaps or deadbands can be incorporated to account for model errors. Thus, model inaccuracy, surface deformation and wear are simply handled.
- The pose estimation process is carried out in a single run. An initialization step using a traditional image-only method is not needed.

Methods

In the traditional method of 3D-to-2D model image registration for joint kinematics measurement, the pose of the each bone or implant is estimated separately. Given the 3D model of an object (a bone or an implant) and the radiographic projection parameters, a computer simulated perspective projection of the 3D model can be generated and compared with the actual x-ray images using an image similarity measure. Given a single frame radiographic image and a 3D model, a search procedure, often a numerical optimization routine, is then used to find the best set of 3D model pose parameters that maximize the similarity measure. This procedure is repeated for each bone or implant and for each frame to obtain the complete temporal kinematics of the bones (Figure 3-1).

Similar to Prins et al. (2010), we combine a penetration computation routine with a numerical optimization routine and simultaneously optimize the image similarity measure and surface penetration. The 12 pose parameters of the articulating bones or implants are optimized together rather than independently.

Penetration Computation Algorithm

Triangle mesh surface models are used due to their simplicity, universal availability and error-free exchangeability between different 3D modeling software packages. Natural bone models are typically obtained by CT or MRI scans and in the form of 3D images. The 3D images can be segmented and transformed into triangle meshes. Implant models are usually 3D CAD models and can be easily exported to triangle mesh models.

Surface penetration/separation is computed based on a point-wise closest distance search using a kd-tree data structure (Bentley, 1975). For each point on one

surface, a query is conducted to determine the closest point on the other surface. The relative orientation of the two triangles and the outward-facing normal determines penetration or separation and the distance contribution to the final penetration score (Fig. 3-2). The kd-tree data structure is a space subdivision algorithm specialized for spatial search and proximity query (Bentley, 1975). Given a swarm of spatial points, a single search for the point that is nearest/furthest to a given coordinate has a computational complexity of $O(\log(n))$. For a pair of potentially contacting models in our application, the kd-tree needs to be constructed only once for only one of meshes. If one surface is designated the 'tree-model' and the other the 'non-tree-model', the pseudo-code of the algorithm follows:

Preprocessing step:

Tree_model_centroids = Centroids(triangles_in_the_tree_model)
KDTree = Construct_KDTree(Tree_model_centroids) in the tree-model's local coordinate system.

Contact computation within each iteration of the optimization problem (when estimated poses of the two models are given):

Transform the non-tree-model into the tree-model's coordinate system.
FOR each triangle T in the non-tree model
 FOR every vertex P of triangle T
 C_tree = KDTree_FindClosestPoint(P)
 T_tree = Triangle_corresponding_to "C_tree"
 n = Outward_Normal(T_tree)
 v = P - C_tree (i.e. the vector connecting C_tree to P)
 IF Dot_product(n, v) < 0
 Conclude P is inside the surface of the tree-model (Fig. 3-2, P1)
 ELSE
 Conclude P is outside the surface of the tree-model (Fig. 3-2, P2)
 ENDIF
 ENDFOR
 Calculate penetration score contribution from "T" based on the location of the vertices.
ENDFOR

Penetration depth, area, quasi-volume or separation distance are readily computed using this approach. On a PC workstation with Intel Xeon 2.4GHz CPU and Windows XP SP3, the contact computation function takes roughly 0.2s to complete with a pair of 3D models of 5000 triangles each.

Image Comparison Metric

The image similarity measure is a measure of distances between the object contour in the actual fluoroscopic image and the contour of the synthetically projected object. First, edge pixels are identified using a Canny edge detector (Canny, 1986) in the actual fluoroscopic image and in the synthetic image. An image mask is created by dilating the edge image of the synthetic image by 25 pixels. The mask is then applied to the edge image of the actual x-ray image to keep only the nearby edge pixels. For each remaining edge point, the closest (in the sense of image coordinates) contour pixel in the artificial projection image is identified and the distance recorded. A second closest point search is performed to find the distance of this point to its nearest edge pixel in the edge image of the actual x-ray image. This distance forms the basis of the contour similarity measure. The final image similarity measure is the sum of squares of all such distance values.

Optimizers and Cost Functions

The surface penetration measure can be incorporated into the registration procedure by adding the penetration score as a penalty to the image similarity measure or as an optimization constraint. Three representative combinations of optimization routines and registration metrics were evaluated. No pre-optimization step was needed for any of the three methods.

Particle swarm pattern search (Pswarm): Particle swarm pattern search (Vaz and Vicente, 2007) combines a stochastic particle swarm global optimization routine with the search/poll structure of local pattern search methods. The algorithm only supports box-bound constraints, so the articular surface penetration function only could be integrated as an augmented penalty function with the image similarity metric. The scalar penetration measure was squared and added to the image similarity measure to form the final cost function for optimization:

$$Cost(x) = (\alpha \cdot p(x))^2 + \sum_i d_i(x)^2 \quad (\text{Eq. 3-1})$$

where x is the 12 pose parameters of the two articulating objects, $p(x)$ is the penetration measure, $\sum d_i(x)^2$ is the image comparison metric as described earlier (sum of squares of edge pixel distances), and the weighting factor α was determined empirically (50 when p is penetration depth). The swarm size was set to 20, and default values for other parameters were used (cognitial parameter = social parameter = 0.5, initial inertia = 0.9, final inertia = 0.4).

RALG optimizer (OpenOpt, version 0.29, National Academy of Sciences of Ukraine, <http://openopt.org/ralg>): RALG is a non-linear/non-smooth problem solver based on Shor's r-algorithm (Shor, 1985), and is a gradient-based deterministic local optimizer. A penalty approach exactly the same as used for the particle swarm optimization was tested. In a second approach, the penetration function was integrated into the optimization as a user supplied constraint function. When supplying the penetration function as a constraint, it was found that scaling in the magnitude of the constraint function affected success rate, and the function value was scaled with a weight of 1e-6. To provide the first derivatives of the cost function and the constraint

function to the optimizer, numerical forward differentiation was performed with a differentiation step size of 0.3mm or 0.3°.

Nonlinear least squares optimization (LSQ): The Levenberg-Marquardt nonlinear least squares algorithm takes as input a vector of errors. As a result, the penetration function could be added as one or more additional elements in the error vector. This is a penalty approach. The vector of image comparison errors was taken as the original point-wise contour distances before taking sum of squares. The penetration penalty was appended to the error vector with a weight such that taking the sum of squares would result in the exact cost function used with the other two optimizers. Numerical forward differentiation was carried out with a differentiation step size of 0.3mm or 0.3° to generate the required Jacobian matrix.

A full list of the optimizer parameter values used can be found in Appendix A.

Experimental Setup

Thirty bi-plane image pairs, reverse engineered 3D knee implant models, and bi-plane kinematic measurements were obtained from Prins et al. (2010). The same dataset was used to evaluate our methods, and their bi-plane measurements were taken as the reference measurements.

Single-plane registration was performed using each of the three methods as described earlier, with and without the surface penetration function. A standard set of initial poses was generated by adding uniform random perturbations of $\pm 2\text{mm}$ for in-plane translations, $\pm 3\text{mm}$ for out-of-plane translations, $\pm 3^\circ$ to the reference measurements. This set of perturbed poses was used as the initial guess for all single-plane registrations. Model-image registration was performed for each model in each

frame. No correction or repeat registration was performed on any of the matching results. For the deterministic RALG and least-squares optimizers, one single run was performed. For the stochastic particle swarm pattern search, 10 runs were performed using different random seeds for the initial particles.

Registration algorithm performance was quantified using success rate and accuracy. The success rate was defined as the percentage of successful registrations on a frame-by-frame basis. A frame qualified as an unsuccessful registration if, compared to the reference measurements, the estimated absolute pose of either the femur or tibia implant model had an error of larger than 1 mm of in-plane translation, 2° in X and Z rotation, or 3° in Y rotation. (For the tibia component, Y rotation corresponds to the rotation about the long axis of the tibia, which is more difficult to measure accurately.) Accuracy was parameterized as mean, standard deviation and root-mean-square (RMS) errors in the measured joint kinematics compared to the reference kinematics. When computing the error statistics, only poses in successfully registered frames were included in the population.

The RALG and particle swarm optimizers were allowed to run for 1000 cost function evaluations. The nonlinear least squares optimizer typically converged within 500 cost function evaluations. In the image-only registrations without contact functions, the femur and tibia components were registered separately. To allow for a fair comparison with the contact-enabled methods, maximum iteration limits were set at 500 cost function evaluations, and in the case of the particle swarm optimizer, swarm size was also reduced by half to 10.

All registrations were performed using custom open-source software (JointTrack, www.sourceforge.net/projects/jointrack). The penetration computation algorithm was implemented as a JointTrack component in C++ using a third party kd-tree implementation (CGAL, Computational Geometry Algorithms Library, <http://www.cgal.org/>). Registration routines and other algorithms were implemented or connected to JointTrack in either C++ or Python, using available third party libraries when possible.

Results

Inclusion of surface penetration penalties or constraints improved the success rate and/or the out-of-plane translation accuracy for all three methods (Table 3-1, Figs. 3-3 and 3-4). Inclusion of surface interactions had no or little effect on the success rate for the nonlinear least-squares method, but resulted in 7% improvement for the RALG method. Significant improvements in out-of-plane translation precision were observed for each of the three methods when using a penetration function (F-test, $p < 1e-10$ for all three methods). X-axis translations (in-plane) were halved when contact constraints were included. Inclusion of surface penetration had little effect on the other four degrees of freedom, changing RMS errors by a maximum of 0.1mm or 0.2°.

Discussion

Model-image registration techniques provide important kinematic measurements for joint biomechanics studies. These techniques often are applied for single-plane radiographic image sequences, where the measurement uncertainties are much greater for out-of-plane translations. When joint surface geometries are known, it is possible to include additional information or constraints to the model-image registration process to improve the out-of-plane measurement accuracy. We showed that model-image

registration with quantified penetration resulted in significantly improved accuracy in the out-of-plane translation compared to image-only registration. In-plane translation accuracy improved as a direct consequence of improved out-of-plane accuracy. Accuracy in the rotational degrees of freedom was comparable between contact-enhanced methods and the standard methods. Similar accuracy was observed for the three numerical methods evaluated.

Evaluation of the surface-enhanced model-image registration techniques was carried out using phantom images and reverse-engineered implant CAD models. These conditions may not capture all of the important features of in vivo images, and therefore may not give a true indication of the utility of these new methods in vivo. However, these new methods were evaluated using the same image dataset and implant models as Prins et al. (2010), so a rigorous quantitative comparison of these related techniques is possible.

Hirokawa's method (Hirokawa et al., 2008) attempt to satisfy a contact constraint for either or both condyles, but does not provide directly a measure of surface separation that would be useful for uncertain or elastic surfaces. The collision detection algorithm used in Prins et al. (2010) is a type of bounding box tree algorithm. This Boolean collision detection algorithm quickly finds intersecting lines between two surfaces but requires additional special data structures and algorithms to obtain the area or volume of penetration. Our contact algorithm, based on the kd-tree data structure, permits fast computation of penetration area and quasi-volume as well as surface separation distances, which could be used to implement ligament-like separation constraints in the future. Hirokawa et al. reported a reduction in out-of-plane

translation errors from approximately 5mm to 1mm using contact constraints. Prins et al. performed a two-step registration procedure and reported a reduction in out-of-plane translation errors from 2.1mm RMS to 0.1mm RMS. Our single-step registration results with and without the contact constraint gave out-of-plane registration errors averaging 2.5mm and 0.5mm RMS, respectively, comparable to the previous reports.

The RALG method performed best in terms of success rate of the three methods incorporating penetration detection. The constraint-function-based RALG optimization resulted in performance similar to penalty-based RALG optimization, but required trial-and-error scaling of the constraint-function to achieve good performance. Scaling sensitivity could have resulted from initial guesses being outside the feasible region defined by the constraints. Constrained optimization algorithms often require initial guesses to be within the feasible region to function correctly, but such a condition is not typically guaranteed in our application.

The non-linear least squares method with edge-based image metric provided the worst success rate but was insensitive to parameter changes, especially changes to contact penalty weighting. Appending 10,000 replicates of the computed penetration to the error vector did not produce a different success rate than appending 100 replicates. In addition, the least squares algorithm does not use or require a box-bound constraint on the search region. The other two algorithms, especially the particle swarm algorithm, demonstrated significantly lower success rates when the box-bound constraint was relaxed. The least squares method also converged quickly, typically in less than 300 function evaluations, while the other two methods required at least twice the number of function evaluations to achieve stable success rate performance.

The particle swarm pattern search algorithm, a stochastic global optimizer, achieved a better success rate than the deterministic non-linear least squares method. However, the particle swarm algorithm is very sensitive to contact penalty weighting and to the bounds supplied for the search region. The reported success rate was the best-case value, and the success rate often fell to lower than 50% when different sets of parameters were used. For best-case success rate, the box-bound constraint was set to exactly the same bounds as were used to generate the perturbed starting positions. It also should be noted that results from global optimizers typically are refined with a local gradient-based optimizer upon completion. We did not include this refinement step, suggesting the results with particle swarm pattern search could be further enhanced.

The present data set utilized a posterior-stabilized implant with a central femoral cam and tibial post, and the choice of contact measure did not produce significantly different results. However, on a posterior-cruciate-retaining implant design lacking a cam-and-post type constraint, registration using the quasi-volume measure significantly outperformed the depth measure in terms of success rate. This will be an important consideration for use of penetration penalties for registration of natural joints, where there is wide variation in articular congruity and lower accuracy in defining the joint surface models. It is reasonable to speculate similar registration penalty functions could be useful with anatomic joints, but additional evaluations need to be conducted to prove this conjecture.

Acknowledgements

The authors thank Andre Prins and Bart Kaptein for generously providing the biplane dataset and reference measurements.

Table 3-1. Success rates and RMS registration errors for three methods with and without the contact function penalty or constraint.

Method	Condition	Success rate	tx (mm)	ty (mm)	tz (mm)	rx (deg)	ry (deg)	rz (deg)
LSQ	no contact	80%	0.7	0.2	2.1	0.4	1.4	0.7
	contact	80%	0.3	0.2	0.6	0.5	1.6	0.7
Pswarm	no contact	88%	0.8	0.2	2.4	0.2	0.6	0.6
	contact	89%	0.4	0.3	0.5	0.2	0.5	0.8
RALG	no contact	90%	0.9	0.2	3.1	0.3	0.8	0.5
	penalty	97%	0.4	0.2	0.3	0.2	0.9	0.6
	constraint	97%	0.4	0.2	0.6	0.3	0.8	0.7

tx and ty represent in-plane translations, tz represents out-of-plane translations; rx, ry and rz represent rotations about the in-plane and out-of-plane axes, respectively. Registration in a frame is unsuccessful if the estimated absolute pose of either the femur or tibia implant model had an error of larger than 1 mm of in-plane translation, 2° in X and Z rotation, or 3° in Y rotation.

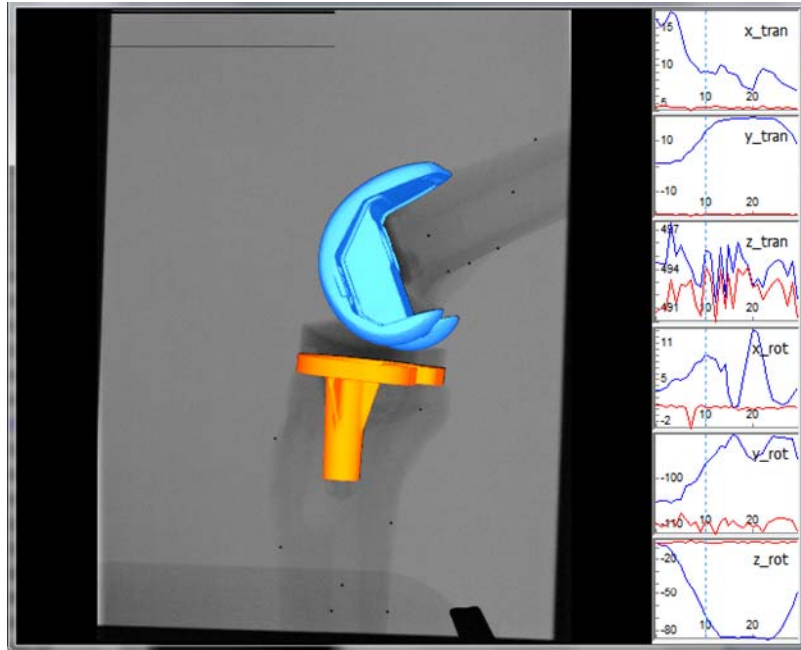


Figure 3-1. Knee implant models matched to the fluoroscopic image to measure their spatial poses.

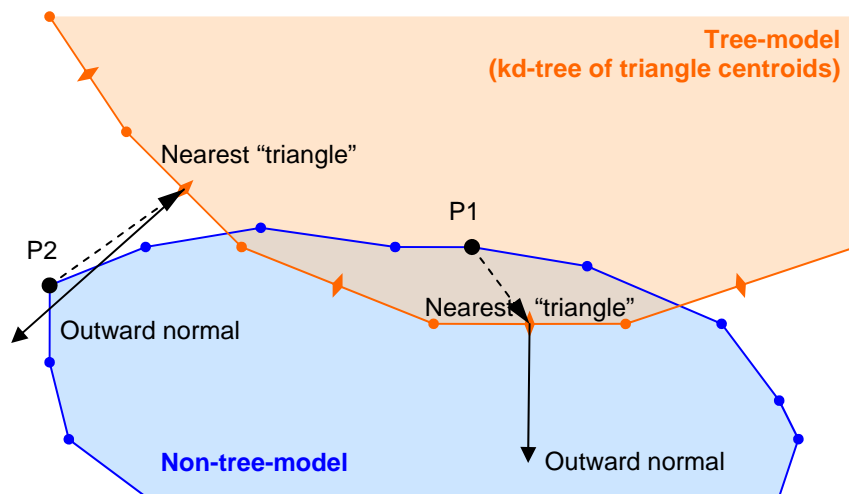


Figure 3-2. Illustration of inside/outside determination for articulating polygonal surfaces. For clarity, the 3D problem is shown as a simplified 2D diagram, where line segments are used to represent triangles and their midpoints are used to represent centroids of triangles.

Error in joint position and joint angles: standard deviation

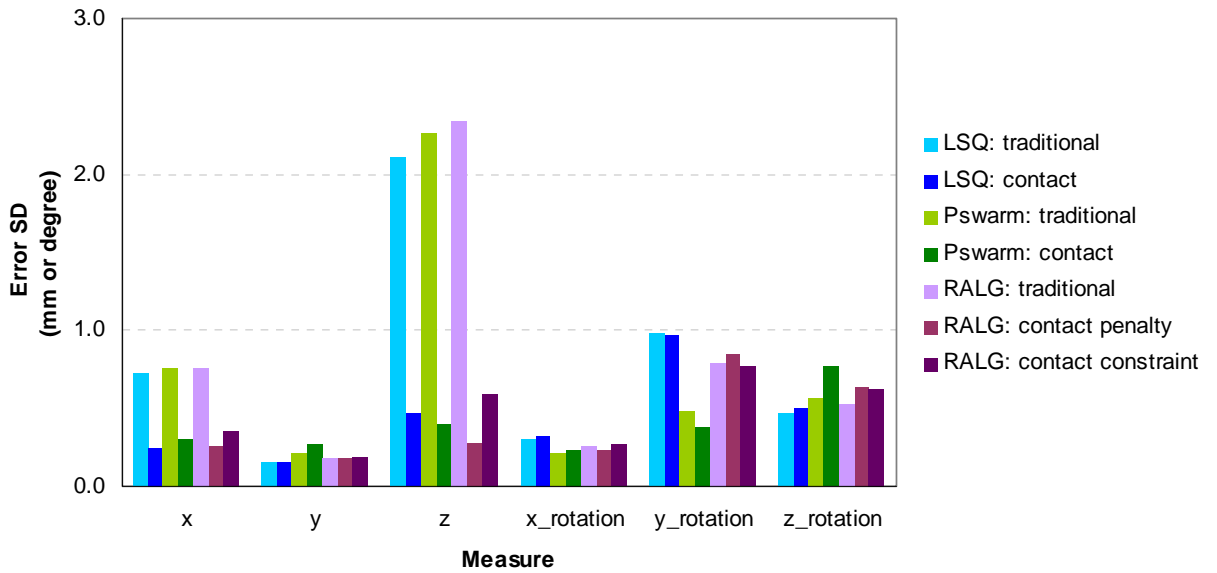


Figure 3-3. Standard deviation of the errors in the measured relative joint position and joint angles.

Error in joint position and joint angles: mean

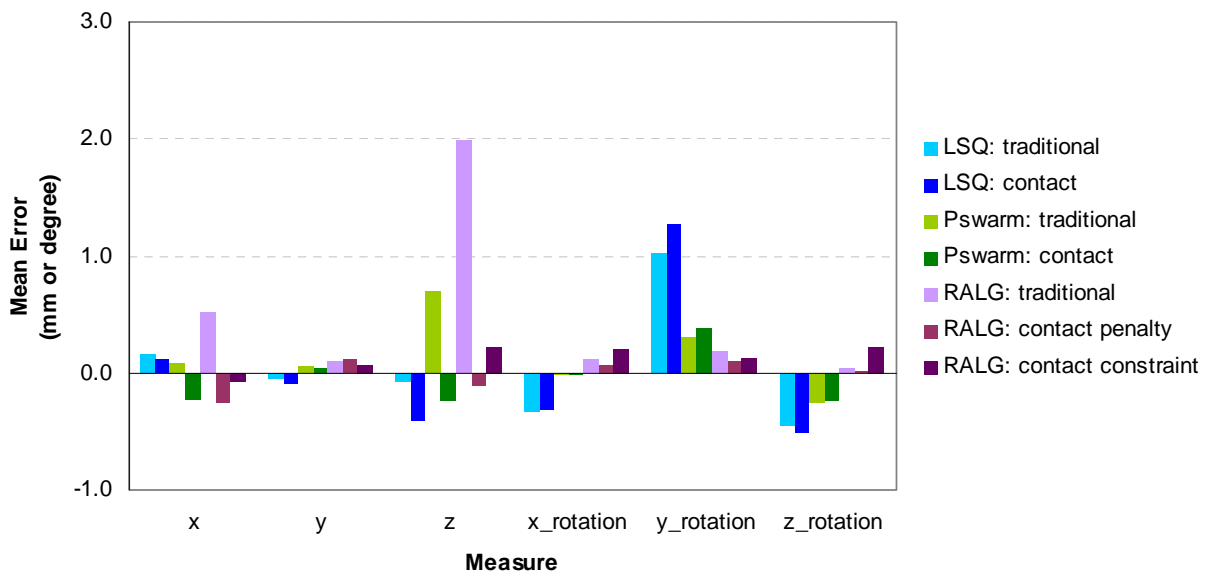


Figure 3-4. Mean errors in the measured relative joint position and joint angles.

CHAPTER 4 LIGAMENT-LIKE JOINT CONSTRAINTS

Introduction

3D-to-2D model-image registration performed with radiographic images is an important tool for measuring in-vivo joint kinematics. It has been proven useful for the study of a number of clinical and research topics in a variety of joints, including knee (Fregly et al., 2005), ankle (Yamaguchi et al., 2009), hip (Tanino et al., 2008), elbow (Matsuki et al., 2010), and shoulder joints (Nishinaka et al., 2008).

In a typical setup, radiographic images of a patient's joint are continuously taken during a motion trial. Poses of the bone or implants in each frame are then measured from the images using the method of 3D-to-2D model-image registration: Given the 3D model of an object (a bone or an implant) and the radiographic projection parameters, a computer simulated perspective projection of the 3D model can be generated and compared with the actual x-ray images using an image similarity measure. Given a single frame radiographic image and a 3D model, a search procedure, often a numerical optimization routine, is then used to find the best set of 3D model pose parameters that minimize (or maximize) this similarity measure. The complete temporal kinematics of the bone is obtained by performing this procedure for all image frames in the trial (Figure 4-1, Right).

A phenomenon often present in the single plane 2D-3D registration task is the symmetric view problem (Figure 4-1). In such situations, a choice must be made according to the object's relationship with other non-symmetric objects whose orientations are much easier to determine. This represents an extreme case of the local minima problem – where there are two equally good choices based on the registration

criteria. The general registration problem is not simple, as typical cost-functions exhibit many local minima and/or long narrow valleys, which depend on the shape and pose of the object, the image similarity measure, features in the image and image quality. Optimization procedures generally are not able to find the correct solution without a very good initial alignment provided by a human operator. When a symmetric view problem is present, even human operators sometimes fail to give correct initial guesses.

Another problem intrinsic to single-plane monocular measurements is the high uncertainty in out-of-plane translation. Hirokawa et al. (2008), Prins et al. (2010) and our group have introduced methods to incorporate articular surface proximity measurements to the traditional image-only registration methods, and achieved improved out-of-plane measurement accuracy. These methods, however, are only effective when a relatively good initial guess is given or after a preliminary registration step.

Human joints are not simply bones. Soft tissues, especially ligaments, play an important role in constraining the motion of a joint and provide a useful framework for additional registration constraints. In this study, we exploit this knowledge and incorporate ligament-like constraints in the registration algorithm and characterize registration performance improvements compared to techniques without such constraints.

Methods

Data Sets

Two total knee arthroplasty data sets were used to evaluate the performance of our methods. The first data set (Dataset A) consists of 47 single-plane fluoroscopic images of a patient's knee in a stair-up motion. The second data set (Dataset B) is 18

images in a walking motion. The total knee implants in the two datasets were cemented posterior cruciate ligament retaining prostheses of different designs from different manufacturers, and their corresponding 3D CAD models were obtained from the manufacturers.

The joint kinematics in both datasets were previously measured using custom software by experienced human operators, using a traditional image-similarity-only registration method. Significant operator supervision was required for the measurement process, and measurement error in the out-of-plane direction was visually corrected by the operator using side views of the 3D models. Results from dataset A were previously used for joint contact and wear modeling (Fregly et al., 2005), and results from dataset B were cross-validated with readings from force sensors instrumented in the tibial component of the knee implant (Zhao et al., 2007). These kinematic measurements were used as the reference kinematics for evaluation of new methods.

Registration Method

The new method minimized a combination of image similarity measure, surface penetration, and ligament force. The surface penetration measure and ligament force were incorporated into the registration procedure as penalties to the image similarity measure. The twelve pose parameters of the femoral and tibial components were optimized together rather than independently for each object.

Surface penetration: Penetration volume (mm^3) between the femur component and the tibial polyethylene insert was estimated using the method described in Chapter 3. For dataset A, the retrieved tibial insert showed creep on its contact surface, so a dead band of 1mm depth was specified in computing the penetration. Penetration

volume to the 0.7 power was used as the penalty score to reduce the cost function's sensitivity to deep penetration.

Ligament force: Ligament forces limit the knee joint's range of motion. We first defined bounds that represent the normal range of motion of the knee joint. Ligament forces are modeled as linear or torsional springs with linear force-displacement relationships. The springs are active only when the estimated poses produce joint translations or joint rotations exceeding the predefined bounds. The bounds are defined as 30 mm femoral posterior translation to 10 mm anterior translation, -5 to 5 mm in medial-lateral translation, -20° to 20° in internal-external rotation, -3° to 3° in varus-valgus angle, and 10° hyperextension to 150° flexion. For dataset A, no active bounds are defined in the relative superior-inferior position between femur and tibia. For dataset B measured forces showed both femoral condyles always to be in contact, so a superior-inferior virtual spring was constantly loaded, pulling the femur and the tibia together.

Image metric: The scalar image similarity measure was the sum of normalized cross-correlations between grayscale and edge images (Canny, 1986), comparing the actual fluoroscopic image and the computer synthesized radiographic projection.

The optimization routine we used is the RALG optimizer (OpenOpt, version 0.29, National Academy of Sciences of Ukraine, <http://openopt.org/ralg>). RALG is a non-linear / non-smooth problem solver based on Shor's r-algorithm (Shor, 1985). To provide the first order partial derivatives of the cost function to the optimizer, numerical forward differentiation was performed with a differentiation step size of 0.3mm for in-plane translations, 0.9mm for out-of-plane translation, 0.6° for y rotation, and 0.3° for x and z

rotations. The differences in these step sizes resulted from the scaling of pose parameters to adjust the cost function's sensitivity in different directions.

For Dataset A, the 12 degrees of freedom being optimized consisted of the absolute poses of the femur and tibia components. A single image similarity score was computed in each cost function evaluation using a computed projection of both components. In the combined cost function the image metric has unit weighting, the ligament force penalties are summed across all directions with a penalty-displacement relation of 0.002 mm^{-1} or 0.002 deg^{-1} , and the penetration penalty has a weight of 0.0002. The image metric has a theoretical range of -1 to +1, but typically takes a value between -0.3 and 0 when a fair initial guess is provided.

Dataset B was more challenging due to the presence of the transmitting and receiving antennae being placed at the anterior tibia in direct apposition to the projected tibial implant. For Dataset B, the absolute pose of the femoral component and the tibial component's pose relative to the femoral component were optimized. A femoral image score and a tibial image score were combined to form a total image score with a relative weighting of 2:1. Compared to Dataset A, weights of the penalty functions were increased by a factor of 10, i.e. 0.02 mm^{-1} or 0.02 deg^{-1} for ligament penalties and 0.002 for the penetration penalty. In addition, the registration process was divided into two stages for Dataset B: the first stage did not include in the cost function the surface penetration measure or the loaded pseudo-ligament in the proximal-distal direction; a second stage optimization started from the results of the first stage, and used all the surface penetration and ligament-like penalties.

Performance Evaluation

Single-plane registration was performed using three methods: image-metric-only registration, registration with image metric and surface penetration penalty, and registration with image metric, surface penetration metric, and ligament-like force metric. Three sets of initial poses were generated by adding uniform random perturbations to the reference measurements. These sets of perturbed poses were used as initial guesses for all registrations.

Due to the shape of total knee implants, the femoral component pose is typically easier and more accurately measured than the tibial component pose; it is also easier for a human operator to align the femoral model with the actual image to give initial guesses to the optimization procedure. Therefore, for the femoral component, the size of the perturbations was set at $\pm 3\text{mm}$ for in-plane translations, $\pm 20\text{mm}$ for out-of-plane translations, and $\pm 5^\circ$ for rotations. For the tibia component, only in-plane translations and in-plane rotation are easy to determine, so the perturbation size was $\pm 3\text{mm}$ for in-plane translations, $\pm 50\text{mm}$ for out-of-plane translation, $\pm 5^\circ$ for in-plane rotation, and $\pm 10^\circ$ for out-of-plane rotations.

Model-image registration using each method was performed for each model in each frame using three sets of initial guesses. No correction or repeat registration was performed on any of the matching results. The optimization routine was allowed to run for 70 iterations (in case of Dataset B, 40 and 30 iterations for the two stages respectively), which was roughly 1200 cost function evaluations including evaluations to compute the derivatives. In the image only registrations without contact or ligament

functions, the femur and tibia implants were registered separately, and maximum iteration limits were set at 35 evaluations.

Registration algorithm performance was quantified using success rate, which was defined as the percentage of successful registrations on a frame-by-frame basis. A frame qualified as an unsuccessful registration if, comparing to the reference measurements, the estimated absolute pose of either the femur or tibia implant model had a deviation of larger than 1.5mm of in-plane translation, 3° in X and Z rotation, or 5° in Y rotation. For the tibia component, Y rotation corresponds to the rotation about the long axis of the tibia, which is typically very difficult to measure accurately (Figure 4-2).

Relative joint kinematics were computed from the measured femur and tibia poses, and their deviations from the values computed from the reference measurements were quantified using root-mean-square (RMS) values. Only measurements from successfully registered frames were included in the population.

Results

Inclusion of the ligament-like force penalty and articular surface penetration metrics resulted in 24% and 46% improvement on the success rate for Dataset A and Dataset B, respectively, compared to image-only registration (Table 4-1). Inclusion of the ligament-like force penalty and articular surface penetration metrics resulted in 31% and 70% improvement on the success rate for Dataset A and Dataset B, respectively, compared to image-plus-contact registration. Compared to the results of the new method, errors in the relative medial-lateral position (z position) were an order of magnitude larger for the traditional image-only registration. Large deviations in the x and y positions resulted from large errors in the out-of-plane translation measurements, due

to the fact that the knee joint's medial-lateral axis was not perfectly aligned with the direction of the x-ray projection in either dataset.

Discussion

Model-image registration techniques provide important kinematic measurements for joint biomechanics studies. These techniques have the common issue of reduced success rate when the initial guesses are not carefully given, or when the images are of bad quality lacking distinct features. We showed that model-image registration augmented with quantified ligament-like forces and articular surface penetration resulted in significantly improved success rate compared to image-only registration. We used two datasets with distinct registration challenges, and showed significant improvements in registration performance with inclusion of ligament-like force penalties.

Images in Dataset A have high contrast and the cement was not visible (Figure 4-1 and 4-3). However, there are certain properties of the tibia components that sometimes trap the optimization into a region far from the real solution (e.g. erroneous results in Figure 4-3). The new method was able to increase the rate of successful registrations. Ligament-like force penalties were not active when the estimated poses were within the natural limits of the knee joint, and hence would not affect the accuracy of successful measurements. Their primary role was to guide the solution search procedure into the region where other techniques, especially the surface contact augmented techniques, effectively function and produce accurate measurements.

In Dataset B the image quality was poor, the external antennae partially block the tibial component projection, the image is low resolution (which creates difficulties for the edge detection algorithm), and an edge line just below the top part of the true tibial component silhouette creates a local minimum in the image similarity metric very close

to the true solution (Figure 4-4). The main objective in this case was to prevent the tibia model from getting trapped in any of the nearby strong local minima. In the first stage optimization without surface-penetration penalties, the ligament-like penalties helped to avoid local minima relatively far from the true solution. In the second stage, a virtual ligament force was added to pull the tibia model against the femur implant and escape spurious local minima. To prevent this force from erroneously “correcting” the femur pose rather than correcting the tibia pose, the tibial component’s relative pose to the femur rather than its absolute pose was optimized. By doing so, a change in only the femur’s pose parameters does not cause a change in the relative pose between the femur and tibia, and therefore does not increase the surface penetration or ligament force penalties. This transformation essentially shapes the cost function and its numerically estimated partial derivatives in favor of the direction search mechanism of the optimizer. However, a side effect is the pose parameters for the femur implant become harder for the optimizer to estimate because any change would affect the perspective projection of both the femur and tibia models. The image matching score due to the femur model projection were therefore given heavier weight than the tibia projection to alleviate this issue. Compared to Dataset A, a much higher weight from the penalty functions was also used. By utilizing these strategies, we significantly reduced the chance of the tibial model getting stuck in the local minimum.

Conceptually, one may argue surface penetration alone could also correct these problems with local minima. However, we showed that the surface penetration measure actually degraded performance without a very good initial guess (Table 4-1,

'image+contact' cases). Although joint limit constraints overlap with contact constraints to a certain degree, each has separate and complementary roles.

This study is the first step to explore different force-type penalties for model-image registration. Many potential alternatives have not yet been explored. For example, we did not evaluate the ligament force constraint without the surface penalty measure. This will be an important alternative, because it is much easier to specify motion constraints with ligament-like penalties than it is to measure or obtain accurate surface geometry to enable surface penetration constraints. We did not evaluate different stiffness values or varying stiffness values for each degree of freedom. A sensitivity study would provide guidance as to how best to use ligament-like constraints for specific types of imaging studies (i.e. knees will likely be different from shoulders).

We have shown in this study that a ligament-like constraint model could be utilized to improve accuracy and the registration success rate when crude initial guesses are given, and to significantly reduce erroneous local solutions when using a carefully chosen optimization strategy. The ultimate goal of all these efforts is to provide a measurement technique that requires minimal user intervention. Inclusion of ligament-like registration penalties significantly reduces the need for accurate initial pose estimates, but does not eliminate the need for human assistance or supervision for robust model-image registration for skeletal kinematic measurements.

Table 4-1. Success rates and the relative pose RMS deviations for two datasets with and without contact and/or ligament penalty.

Dataset	Method	Success rate	Position (mm)			Orientation (°)		
			x	y	z	x	y	z
A	image	55%	4.7	1.6	15.9	0.9	2.4	1.2
	image+contact	48%	4.8	1.6	16.3	0.8	2.3	1.2
	image+contact+ligament	79%	0.8	0.4	1.7	0.7	1.3	1.0
B	image	28%	1.0	1.1	12.6	1.3	2.8	1.1
	image+contact	4%	2.4	1.8	29.5	2.1	3.9	0.7
	image+contact+ligament	74%	1.1	0.4	3.8	0.4	1.9	1.7

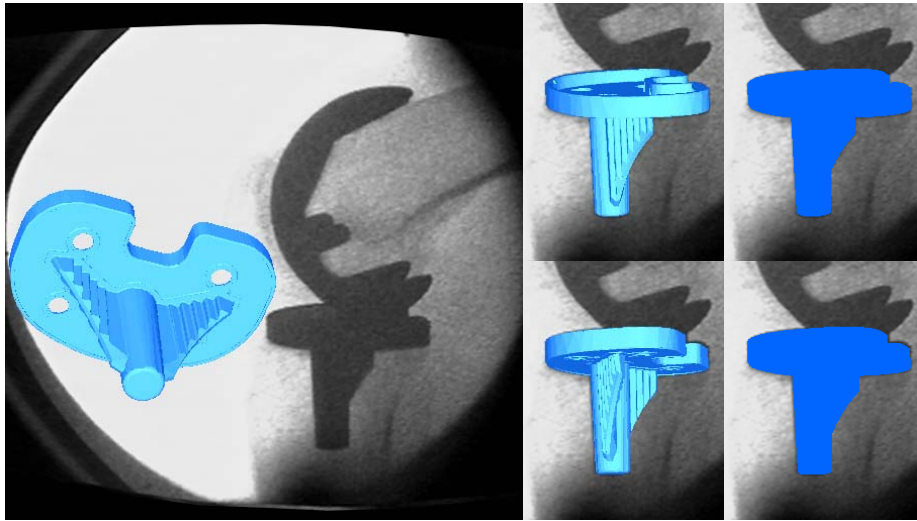


Figure 4-1. The symmetric view problem involves nearly equivalent projections of symmetric objects.

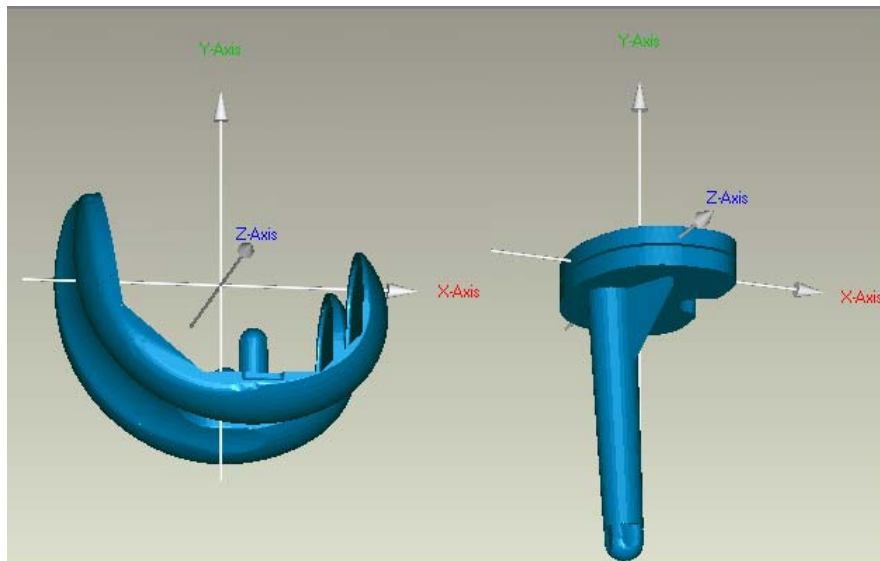


Figure 4-2. Coordinate system definition for the femoral and tibial implant models.

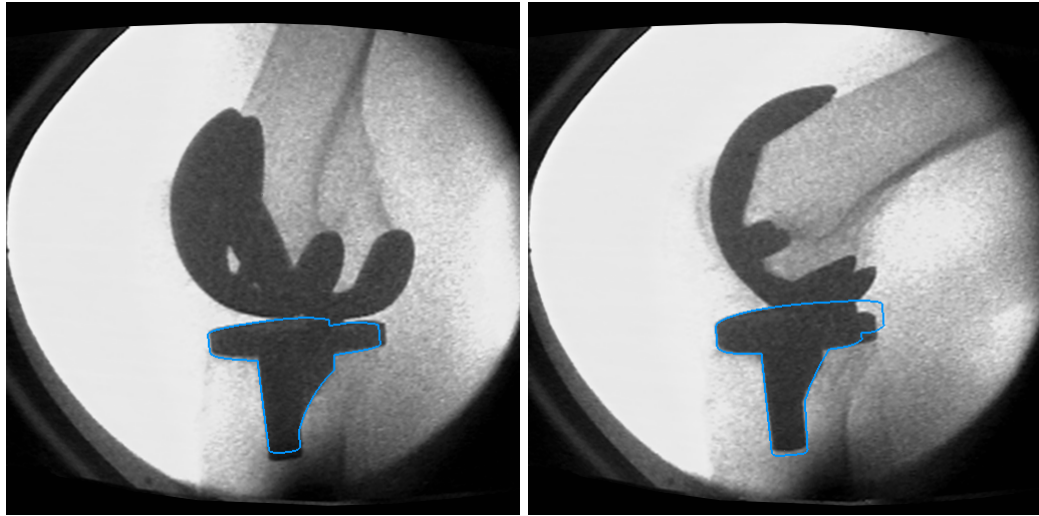


Figure 4-3. Silhouette of ill-registered tibia component models. The right side error is a case of semi-symmetrical view.

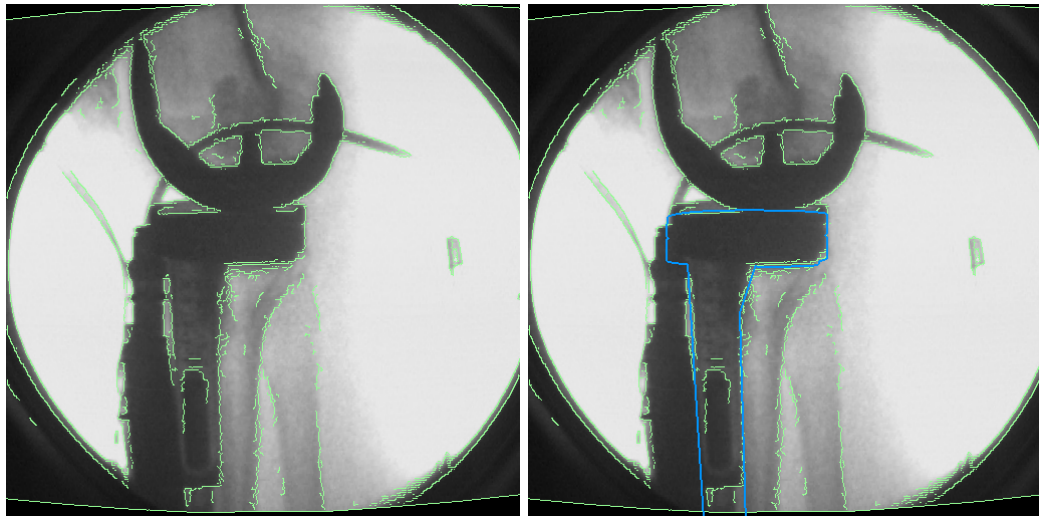


Figure 4-4. An image from Dataset B. Left: Edges identified by a Canny edge detector were superimposed on top of the image. Right: Silhouette of the tibia component model whose top contour was erroneously registered with the wrong edge.

CHAPTER 5 CONCLUSION

3D-to-2D model-image registration is increasingly used by researchers worldwide for skeletal kinematic measurement. The method has proven utility in many situations where alternatives for quality kinematics are few. However, there remain a number of technical issues requiring improvement, and the key obstacle to wider adoption remains the significant human intervention required to provide initial guesses for registration. We investigated several methods to address these issues, and demonstrated better accuracy and success rates.

Typical model-image registration techniques estimate the pose of each object separately. We showed significant improvement by estimating all objects poses together using additional domain-specific knowledge. Increasing the dimensionality of the problem may seem counter-intuitive, but in doing so we divided the problem into a coarse large-error rejection problem and a fine precision measurement problem, which makes better use of available information. We showed that an image similarity measure alone is useful for all conditions but insufficient to robustly solve any of them.

Future work should address how to obtain initial pose estimates when no human-provided initial guess is given. Human beings learn, identify and reproduce the rough position and orientation of objects easily and quickly. A machine learning approach might be appropriate for this purpose. In fact, a former lab member performed preliminary work with the SIFT (Scale Invariant Feature Transform) classifier and obtained some promising results. Whether this approach provides the required accuracy in all directions for our existing methods to function effectively remains unknown.

We showed the success rate with any method is less than 100%. Further work is necessary to address this issue as operator verification and correction still requires a significant amount of human intervention. As shown in Chapters 2 and 4, image quality, image modality, and object geometric properties have a dramatic effect on measurement accuracy and success rate. Advanced image analysis techniques and utilization of artificial digitally reconstructed radiographs (DRRs) are needed.

The new methods we presented here provide improved accuracy and robustness, making 3D-to-2D model-image registration an increasingly superior technique compared to traditional 2D image measurements or other invasive or skin-marker-based techniques for skeletal kinematic measurements. These new techniques and tools are now readily available for use by researchers in our Orthopedic Biomechanics Laboratory at the University of Florida, as well as researchers worldwide through the free distribution of the JointTrack program.

APPENDIX
OPTIMIZER PARAMETER VALUES

Table A-1. Particle swarm pattern search parameter values.

Parameter	Description	Value
s	swarm size	20
mu	cognitial parameter	0.5
nu	social parameter	0.5
maxvfactor	maximum velocity factor	0.5
Maxiter	maximum number of iterations	50
Maxf	maximum of function evaluations	1000
iweight	initial inertial weight	0.9
fweight	final inertial weight	0.4
tol	x tolerance for stopping criteria	1.0E-05
idelta	pattern search mesh size expansion factor	2
ddelta	pattern search mesh size reduction factor	0.5

Table A-2. RALG optimizer parameter values.

Parameter	Value
alpha	2.0
h0	1.0
nh	3
q1	0.9
q2	1.1
hmult	0.5
S	0
dilationType	plain difference
doBackwardSearch	True
xTolerance	0.01

For the meaning of the parameters, please refer to Shor (1985) and Kappel and Kuntsevich (2000).

Table A-3. Levenberg-Marquardt nonlinear least squares optimizer parameter values.

Parameter	Description	Value
ftol	relative error desired in the sum of squares	1.5e-08
xtol	relative error desired in the solution	1.5e-08
gtol	orthogonality desired between the function vector and the columns of the Jacobian	0.0
maxfev	maximum of function evaluations	1000

LIST OF REFERENCES

- Banks, S., Hodge, W., 1992. 3D knee prosthesis kinematics from single plane fluoroscopy. *Orthopaedic Transactions* 16(2), 530.
- Banks, S.A., Fregly, B.J., Boniforti, F., Reinschmidt, C., Romagnoli, S., 2005. Comparing in vivo kinematics of unicondylar and bi-unicondylar knee replacements. *Knee Surgery, Sports Traumatology, Arthroscopy* 13(7), 551-556.
- Banks, S.A., Hodge, W.A., 1996. Accurate measurement of three-dimensional knee replacement kinematics using single-plane fluoroscopy. *IEEE Transactions on Biomedical Engineering* 43(6), 638-649.
- Banks, S.A., Markovich, G.D., Hodge, W.A., 1997. In vivo kinematics of cruciate-retaining and -substituting knee arthroplasties. *The Journal of Arthroplasty* 12(3), 297-304.
- Banks, S.A., Riley, P.O., Spector, C., Hodge, W.A., 1991. In vivo bearing motion with meniscal bearing TKR. *Orthopaedic Transactions* 15(2), 544.
- Bentley, J.L., 1975. Multidimensional binary search trees used for associative searching. *Communications of the ACM* 18(9), 509-517.
- Bey, M.J., Kline, S.K., Tashman, S., Zauel, R., 2008. Accuracy of biplane x-ray imaging combined with model-based tracking for measuring in-vivo patellofemoral joint motion. *Journal of Orthopaedic Surgery and Research* 3, 38.
- Canny, J., 1986. A Computational Approach to Edge-Detection. *IEEE Transactions on Pattern Analysis and Machine Intelligence* 8(6), 679-698.
- Fregly, B.J., Sawyer, W.G., Harman, M.K., Banks, S.A., 2005. Computational wear prediction of a total knee replacement from in vivo kinematics. *Journal of Biomechanics* 38(2), 305-314.
- Goffe, W.L., Ferrier, G.D., Rogers, J., 1994. Global Optimization of Statistical Functions with Simulated Annealing. *Journal of Econometrics* 60(1-2), 65-99.
- Hirokawa, S., Abrar Hossain, M., Kihara, Y., Ariyoshi, S., 2008. A 3D kinematic estimation of knee prosthesis using X-ray projection images: clinical assessment of the improved algorithm for fluoroscopy images. *Medical & Biological Engineering & Computing* 46(12), 1253-1262.
- Kappel, F., Kuntsevich, A.V., 2000. An implementation of Shor's r-algorithm. *Computational Optimization and Applications* 15(2), 193-205.

Kaptein, B.L., Valstar, E.R., Stoel, B.C., Reiber, H.C., Nelissen, R.G., 2007. Clinical validation of model-based RSA for a total knee prosthesis. *Clinical Orthopaedics and Related Research*(464), 205-209.

Kaptein, B.L., Valstar, E.R., Stoel, B.C., Rozing, P.M., Reiber, J.H.C., 2003. A new model-based RSA method validated using CAD models and models from reversed engineering. *Journal of Biomechanics* 36(6), 873-882.

Kirkpatrick, S., Gelatt, C.D., Vecchi, M.P., 1983. Optimization by Simulated Annealing. *Science* 220(4598), 671-680.

Komistek, R.D., Dennis, D.A., Mahfouz, M., 2003. In vivo fluoroscopic analysis of the normal human knee. *Clinical Orthopaedics and Related Research*(410), 69-81.

Komistek, R.D., Dennis, D.A., Ochoa, J.A., Haas, B.D., Hammill, C., 2002. In vivo comparison of hip separation after metal-on-metal or metal-on-polyethylene total hip arthroplasty. *Journal of Bone and Joint Surgery-American Volume* 84A(10), 1836-1841.

Kon, Y., Nishinaka, N., Gamada, K., Tsutsui, H., Banks, S.A., 2008. The influence of handheld weight on the scapulohumeral rhythm. *Journal of Shoulder and Elbow Surgery* 17(6), 943-946.

Lavallee, S., Szeliski, R., 1995. Recovering the position and orientation of free-form objects from image contours using 3D distance maps. *IEEE Transactions on Pattern Analysis and Machine Intelligence* 17(4), 378-390.

Li, G., Papannagari, R., Nha, K.W., DeFrate, L.E., Gill, T.J., Rubash, H.E., 2007. The coupled motion of the femur and patella during in vivo weightbearing knee flexion. *Journal of Biomechanical Engineering-Transactions of the Asme* 129(6), 937-943.

Li, G., Wuerz, T.H., DeFrate, L.E., 2004. Feasibility of using orthogonal fluoroscopic images to measure in vivo joint kinematics. *Journal of Biomechanical Engineering* 126(2), 314-318.

Mahfouz, M.R., Hoff, W.A., Komistek, R.D., Dennis, D.A., 2003. A robust method for registration of three-dimensional knee implant models to two-dimensional fluoroscopy images. *IEEE Transactions on Medical Imaging* 22(12), 1561-1574.

Matsuki, K.O., Matsuki, K., Mu, S., Sasho, T., Nakagawa, K., Ochiai, N., Takahashi, K., Banks, S.A., 2010. In vivo 3D kinematics of normal forearms: Analysis of dynamic forearm rotation. *Clinical Biomechanics* doi:10.1016/j.clinbiomech.2010.07.006.

McDonald, C.P., Bachison, C.C., Chang, V., Bartol, S.W., Bey, M.J., 2010. Three-dimensional dynamic in vivo motion of the cervical spine: assessment of measurement accuracy and preliminary findings. *Spine Journal* 10(6), 497-504.

Moro-oka, T., Hamai, S., Miura, H., Shimoto, T., Higaki, H., Fregly, B.J., Iwamoto, Y., Banks, S.A., 2007. Can magnetic resonance imaging-derived bone models be used for accurate motion measurement with single-plane three-dimensional shape registration? *Journal of Orthopaedic Research* 25(7), 867-872.

Moro-oka, T., Hamai, S., Miura, H., Shimoto, T., Higaki, H., Fregly, B.J., Iwamoto, Y., Banks, S.A., 2008. Dynamic activity dependence of in vivo normal knee kinematics. *Journal of Orthopaedic Research* 26(4), 428-434.

Nishinaka, N., Tsutsui, H., Mihara, K., Suzuki, K., Makiuchi, D., Kon, Y., Wright, T.W., Moser, M.W., Gamada, K., Sugimoto, H., Banks, S.A., 2008. Determination of in vivo glenohumeral translation using fluoroscopy and shape-matching techniques. *Journal of Shoulder and Elbow Surgery* 17(2), 319-322.

Prins, A.H., Kaptein, B.L., Stoel, B.C., Reiber, J.H., Valstar, E.R., 2010. Detecting femur-insert collisions to improve precision of fluoroscopic knee arthroplasty analysis. *Journal of Biomechanics* 43(4), 694-700.

Shor, N.Z., 1985. Minimization methods for non-differentiable functions, Springer Series in Computational Mathematics, vol. 3. Springer-Verlag: Berlin.

Stiehl, J.B., Dennis, D.A., Komistek, R.D., Crane, H.S., 1999. In vivo determination of condylar lift-off and screw-home in a mobile-bearing total knee arthroplasty. *Journal of Arthroplasty* 14(3), 293-299.

Tang, T.S., MacIntyre, N.J., Gill, H.S., Fellows, R.A., Hill, N.A., Wilson, D.R., Ellis, R.E., 2004. Accurate assessment of patellar tracking using fiducial and intensity-based fluoroscopic techniques. *Med Image Anal* 8(3), 343-351.

Tanino, H., Ito, H., Harman, M.K., Matsuno, T., Hodge, W.A., Banks, S.A., 2008. An in vivo model for Intraoperative assessment of impingement and dislocation in total hip arthroplasty. *Journal of Arthroplasty* 23(5), 714-720.

Tashman, S., Kolowich, P., Collon, D., Anderson, K., Anderst, W., 2007. Dynamic function of the ACL-reconstructed knee during running. *Clinical Orthopaedics and Related Research*(454), 66-73.

Tsai, T.Y., Lu, T.W., Chen, C.M., Kuo, M.Y., Hsu, H.C., 2010. A volumetric model-based 2D to 3D registration method for measuring kinematics of natural knees with single-plane fluoroscopy. *Medical Physics* 37(3), 1273-1284.

Valstar, E.R., de Jong, F.W., Vrooman, H.A., Rozing, P.M., Reiber, J.H., 2001. Model-based Roentgen stereophotogrammetry of orthopaedic implants. *Journal of Biomechanics* 34(6), 715-722.

- Vaz, A.I.F., Vicente, L.N., 2007. A particle swarm pattern search method for bound constrained global optimization. *Journal of Global Optimization* 39(2), 197-219.
- Wang, S., Passias, P., Li, G., Li, G., Wood, K., 2008. Measurement of vertebral kinematics using noninvasive image matching method - Validation and application. *Spine* 33(11), E355-E361.
- Yamaguchi, S., Gamada, K., Sasho, T., Kato, H., Sonoda, M., Banks, S.A., 2009. In vivo kinematics of anterior cruciate ligament deficient knees during pivot and squat activities. *Clinical Biomechanics (Bristol, Avon)* 24(1), 71-76.
- Yamaguchi, S., Sasho, T., Kato, H., Kuroyanagi, Y., Banks, S.A., 2009. Ankle and Subtalar Kinematics During Dorsiflexion-Plantarflexion Activities. *Foot & Ankle International* 30(4), 361-366.
- Yamazaki, T., Watanabe, T., Nakajima, Y., Sugamoto, K., Tomita, T., Yoshikawa, H., Tamura, S., 2004. Improvement of depth position in 2-D/3-D registration of knee implants using single-plane fluoroscopy. *IEEE Transactions on Medical Imaging* 23(5), 602-612.
- You, B.M., Siy, P., Anderst, W., Tashman, S., 2001. In vivo measurement of 3-D skeletal kinematics from sequences of biplane radiographs: application to knee kinematics. *IEEE Transactions on Medical Imaging* 20(6), 514-525.
- Yushkevich, P.A., Piven, J., Hazlett, H.C., Smith, R.G., Ho, S., Gee, J.C., Gerig, G., 2006. User-guided 3D active contour segmentation of anatomical structures: Significantly improved efficiency and reliability. *Neuroimage* 31(3), 1116-1128.
- Zhao, D., Banks, S.A., D'Lima, D.D., Colwell, C.W., Fregly, B.J., 2007. In vivo medial and lateral tibial loads during dynamic and high flexion activities. *Journal of Orthopaedic Research* 25(5), 593-602.
- Zuffi, S., Leardini, A., Catani, F., Fantozzi, S., Cappello, A., 1999. A model-based method for the reconstruction of total knee replacement kinematics. *IEEE Transactions on Medical Imaging* 18(10), 981-991.

BIOGRAPHICAL SKETCH

Shang Mu received his bachelor's degree from Beihang University (Beijing University of Aeronautics and Astronautics), Beijing, China, in 2005. He joined the University of Florida thereafter. Apart from his pursuit in engineering, his biggest interest lies in physics.